VILNIUS UNIVERSITY
STATE RESEARCH INSTITUTE
CENTER FOR PHYSICAL SCIENCES AND TECHNOLOGY

Sergej
ŠEMČUK

Application of graphene oxide based nanocomposites and Šaltiškiai clay for radionuclides removal from contaminated solutions

DOCTORAL DISSERTATION

Physical sciences,
Physics 02P

VILNIUS 2018

Dissertation was prepared at Institute of Physics of the SRI Center for Physical Science and Technology in 2013 – 2017.

Supervisor:
Dr. Galina Lujanienė (SRI Center for Physical Science and Technology, Physical sciences, Chemistry – 03P, Physics – 02P)

VILNIAUS UNIVERSITETAS
VALSTYBINIS MOKSLINIŲ TYRIMŲ INSTITUTAS
FIZINIŲ IR TECHNOLOGIJOS MOKSLŲ CENTRAS

Sergej
ŠEMČUK

Grafeno oksido nanokompozitų ir Šaltiškių molio taikymas šalinant radionuklidus iš skystųjų užterštųjų terpių

Daktaro disertacija

Fiziniai mokslai,
Fizika 02P

VILNIUS 2018

Disertacija rengta VMTI Fizinių ir technologijos mokslų centro Fizikos institute 2013 – 2017 metais.

Darbo vadovas:
dr. Galina Lujanienė (VMTI Fizinių ir technologijos mokslų centras, fiziniai mokslai, chemija – 03P, fizika – 02P)

CONTENT

ABBREVIATIONS

CMG – chemically modified graphene
CNT – carbon nanotubes
CS – chitosan
CSGO – chitosan graphene oxide
FTIR – Fourier-transform infrared spectroscopy
GO – graphene oxide
MGO – magnetic graphene oxide
MPB – magnetic Prussian blue
MPBGO – magnetic Prussian blue graphene oxide
PB – Prussian blue
PBGO – Prussian blue graphene oxide
SE – sequential extraction
SEM – scanning electron microscopy
TEM – tunnel electron microscopy
XRD – X-Ray diffraction

INTRODUCTION

Over the past hundred years, humanity has made a huge leap in development, which has led to the prosperity of all industries. The standard of living has grown in many countries, and, as is known, along with these changes, there is an increase in consumption of resources and energy, as well as pollution of the environment and water.

The low-cost way to produce energy is to use a nuclear power plant, but it cannot provide sufficient security and can cause the pollution of the environment with various radionuclides due to the use of nuclear fuel. Environmental waters are most polluted with heavy metals and radionuclides. Pollutants can persist in nature hundreds or even thousands of years depending on their speciation. The requirements of environmental protection led to the improvement of cleaning technologies and accelerate the development and use of new materials. The most popular methods for water cleaning are based on sorption using various sorbents. This technique causes many problems associated with the selectivity, efficiency and other sorption parameters. Researchers are developing new, low-cost and more eco-friendly sorbents to improve cleaning technologies.

In past two decades, the one of the fastest growing areas of science is the nanoscale materials. Nanosized derivatives are used in various fields: medicine (drugs, sensors, biosensors), electrical engineering, food industry, etc. In addition, huge attention is paid to the synthesis of nanosorbents. The most studied are carbon derivatives and allotropes, including graphen oxide (GO). Researchers became interested in GO again after 2010, when prof. A.K. Geim and prof. K.S. Novoselov received the Nobel Prize in the field of physics for the discovery of the specific properties of the graphene mono layer.

The results of sorption of synthesized graphene oxide and its modified nanosized composites in experiments with radionuclides and metals are presented in this study. Although the conducted studies did not fully demonstrate the potential of sorbents for the treatment of polluted water, but, on the other hand, they made it possible to evaluate the sorption efficiency, properties and reaction mechanisms of the selected sorbents.

The results presented in the thesis can enhance the knowledge of using of nanocomposites for removal of radionuclides from liquid media, be useful for development of new technologies for cleaning contaminated liquids, minimize the consequences of possible accidents in the environment of nuclear power plants and waste storage facilities, and expand the application of composites.

Aim and objectives of the study

The aim of this work was to investigate the potential of graphene oxide, graphene oxide-based nanocomposites and clay minerals for the sorption of radionuclides from solutions in order to apply them to the cleaning of contaminated fluids.

The following goals were formulated to achieve the objectives:

1. To oxidize graphite to graphene oxide and apply it as a base for modifying with Prussian blue, chitosan and magnetite.
2. To investigate the potential of graphene oxide and modified nanocomposites for the sorption of radionuclides from liquid media by conducting sorption experiments with ^{134}Cs (I), ^{60}Co (II), ^{241}Am (III), ^{239}Pu (IV) and ^{239}Pu (V) as well as Cu (II), Co (II), Ni (II) and Pb (II) as stable radionuclide analogues.
3. To determine the equilibrium and kinetic radionuclide sorption parameters at different initial element concentrations in a wide range of pH. To estimate the optimal conditions for radionuclide sorption.
4. To investigate mechanisms of Pu isotope sorption on clay minerals. To determine changes in the Pu oxidation state and its effect on the sorption parameters.

Novelty of the study

1. For the first time chitosan graphene oxide nanocomposite was used for the removal of Am (III) and Pu (IV, V) from liquid media.
2. Graphene oxide (GO) of a higher oxidation level, used as a substrate for the modification of nanocomposites, increased their adsorption efficiency up to 95 % for ^{241}Am and ^{239}Pu isotopes over a wide pH range.

Scientific and practical significance of the results

1. In this work, sorbents synthesized based on the graphene oxide for separation of radionuclides from contaminated waters are studied. In

addition, natural clay was investigated as an alternative sorbent capable removing radionuclide from liquid media. Estimated physical and chemical parameters, affecting the efficiency and kinetics of sorption, are useful for eliminating the consequences of possible accidents in the environment of nuclear power plants and waste storage facilities.

2. Synthesized magnetic Prussian blue graphene oxide nanocomposite demonstrates high absorption efficiency of radioactive Cs (I) from contaminated media.
3. Knowledge about changes in Pu oxidation state and formation of Pu "mobile" species are important for assessing the distribution of Pu (V), not only in the natural environment, but also in the analysis of safety in waste storage areas.

Statements to be defined:

1. During the synthesis of the magnetic graphene oxide nanocomposite, a degree of graphene oxidation determines the amount of the bonded modifier, therefore the sorption efficiency of MGO nanocomposite for radionuclides from the contaminated medium in the pH range from 5 to 9 increases by a factor of 1.3.
2. The efficiency of magnetic Prussian blue graphene oxide (MPBGO) nanocomposites to sorb Cs (I) is the highest in comparison with other sorbents tested in the work and does not change even in the presence of high levels of K^+, Na^+, Ca^{2+}, Mg^{2+} and other ions.
3. The spread of Pu (V) in the environment is due to the association of the element with mineral coatings on the surface of the Šaltiškiai clay and the formation of "mobile" (carbonate and exchangeable) geochemical forms.

Author's contribution:

The author planned the research activities: nanocomposites synthesis, preparation of the samples, sorption experiments and analysis of the experimental data. He also, contributed in the writing of the manuscripts, presented and discussed the results in the conferences.

Scientific approval:

List of publications:

1. Lujanienė G., **Šemčuk S.**, Leščinskytė A., Kulakauskaitė I., Mažeika K., Valiulis D., Pakštas V., Skapas M., Tumėnas S., 2017. Magnetic graphene oxide based nanocomposites for removal of radionuclides and metals from contaminated solutions. *Journal of environmental radioactivity.* 166, 166 – 174;
2. **Šemčuk S.**, Lujanienė G., Tautkus S., Juškėnas R., Laurinavičius D., 2017. Application of graphene oxide and the chitozan-graphene oxide composite for the removal of radionuclides and metals from contaminated solutions. *Proceedings of the 4th international conference on environmental radioactivity "Radionuclides as tracers of environmental processes" (ENVIRA 2017), Vilnius, Lithuania,*133 – 136;
3. Lujanienė G., **Šemčuk S.**, Kulakauskaitė I., Mažeika K., Valiulis D., Juškėnas R., Tautkus S., 2016. Sorption of radionuclides and metals to graphene oxide and magnetic graphene oxide. *Journal of radioanalytical and nuclear chemistry,* 307, 2267 – 2275;
4. Lujanienė G., Štamberg K., Pakštas V., Juškėnas R., Kulakauskaitė I., **Šemčuk S.**, Mažeika K., Vopalka D., 2015. Study of Pu sorption behavior in natural clay. *Journal of radioanalytical and nuclear chemistry,* 304, 53 – 59.

Other publications:

1. Lujanienė G., Povinec P.P., Li H.C., Barisevičiūtė R., Remeikaitė-Nikienė N., Malejevas V., Garnaga-Budrė G., Terrassi F., Pánik J., Kaizer J., **Šemčuk S.,** Jokšas K., Tracevičienė D., Stankevičius A., 2017. Carbon and Pu isotopes in Baltic sea sediments. *Applied radiation and isotopes,* 126, 49 – 53;
2. Lujanienė G., Remeikaitė-NikienėN., Garnaga G., Jokšas K., Šilobritienė B., Stankevičius A., **Šemčuk S.,** Kulakauskaitė I., 2014. Transport of 137Cs, 241Am and Pu isotopes in the Curonian Lagoon and the Baltic Sea. *Journal of environmental radioactivity,*127, 40 – 49;

3. Lujanienė G., Mažeika J., Petrošius R., Remeikaitė-Nikienė N., Barisevičiūtė R., JokšasK., Garnaga G., StankevičiusA., Kulakauskaitė I., **Šemčuk S.,** 2013. Anglies ir plutonio izotopai Baltijos jūros ir Kuršių marių dugno nuosėdose. *Jūros ir krantų tyrimai - 2013: 7-oji mokslinė-praktinė konferencija: konferencijos medžiaga,* 149 – 155.

List of conferences and seminars:

1. **Šemčuk S.,** Lujanienė G., 2017. Study of radionuclides and heavy metals sorption on graphene oxide and chitosan graphene oxide composite. *International Conference on Chemistry and Material Science, October 18-20, Rome, Italy,* 60;
2. Leščinskytė A., Lujanienė G., **Šemčuk S.**, Mažeika K., Juškėnas R., 2017. Application of Prussian blue based nanocomposites for radiocesium pre-concentration from seawater. *4th international conference on environmental radioactivity: Radionuclides as tracers of environmental proceses (ENVIRA 2017), 29 May- 2 June, Vilnius, Lithuania,*148;
3. **Šemčuk S.**, Lujanienė G., Valiulis D., Leščinskytė A., Tautkus S., Laurinavičius D., 2017. Radionuclides and heavy metal removal using chitosan-graphene oxide composite. *4th international conference on environmental radioactivity: Radionuclides as tracers of environmental proceses (ENVIRA 2017), 29 May- 2 June, Vilnius, Lithuania,* 243;
4. Lujanienė G., Levinskaitė L., Juškėnas R., Štamberg K., Kačergius A., Kulakauskaitė I., **Šemčuk S.**, Vodopalka D., 2016. Study of Cs, Pu and Am sorption to natural clay and bottom sediments. *9th international conference on nuclear and radiochemistry, August 29-September 2, Helsinki, Finland,* 65;
5. **Šemčuk S.**, Lujanienė G., Leščinskytė A., Tautkus S., Kulakauskaitė I., Juškėnas R., 2016. Sorption of Cs, Pu and Am to graphene oxide based nanosorbents. *9th international conference on nuclear and radiochemistry, August 29-September 2, Helsinki, Finland,* 179;
6. Leščinskytė A., Lujanienė G., **Šemčuk S.**, Mažeika K., Juškėnas R., 2016. Prussian blue based nanocomposites for radiocesium removal. *International conference of Lithuanian Society of Chemistry "Chemistry and Chemical Technology 2016", April 28-29, Vilnius, Lithuania,* 141;

7. **Šemčuk S.**, Lujanienė G., Leščinskytė A., Tautkus S., Juškėnas R., 2016.Study of radionuclides and heavy metals sorption on GO. *International conference of Lithuanian Society of Chemistry "Chemistry and Chemical Technology 2016", April 28-29, Vilnius, Lithuania,* 142;

8. Lujanienė G., Levinskaitė L., Juškėnas R., Štamberg K., Kačergius A., Kulakauskaitė I., Gavutis M., **Šemčuk S.**, Vopalka D., 2016. Sorption behavior of Cs, Pu and Am to natural clay: effect of various components. *International conference on radioanalytical and nuclear chemistry (RANC-2016), April 10-15, Budapest, Hungary,* 56;

9. Lujanienė G., **Šemčuk S.**, Kulakauskaitė I., Mažeika K., Tautkus S., Valiulis D., Juškėnas R., 2015. Application of graphene oxide and magnetic graphene oxide for removal of radionuclides and heavy metals from contaminated wastewater /*International conference "Environmental radioactivity" (ENVIRA2015), September 21- 25, Thessaloniki, Greece,* 281;

10. Lujanienė G., Kulakauskaitė I., **Šemčuk S.**, Tautkus S., Valiulis D., Mažeika K., Motiejūnas S., 2015. Sorption of radionuclides and heavy metals to natural clay, graphene oxide and graphene oxide-ferrous oxide composite. *Tenth international conference on methods and applications of radioanalytical chemistry (MARC X), April 12-17, Kailua-Kona, USA,* 207;

11. Kulakauskaitė I., Lujanienė G., **Šemčuk S.**, Mažeika K., Tautkus S., 2014. Synthesis and characterization of graphene oxide and graphene oxide-ferrous oxide composite. *Radiation interaction with materials: fundamentals and applications. 5th international conference, May 12-15, Kaunas, Lithuania,* 254 – 255;

12. **Šemčuk S.**, Lujanienė G., Kulakauskaitė I., Tautkus S., 2014. Kinetics of Pu and Am sorption to graphene oxide and graphene oxide-ferrous oxide composite. *Radiation interaction with materials: fundamentals and applications. 5th international conference, May 12-15, Kaunas, Lithuania,* 256 – 257;

13. Lujanienė G., Juškėnas R., Levinskaitė L., Kulakauskaitė I., Gavutis M., **Šemčuk S.**, 2013. Pu oxidation state transformation by natural clay and their various component. *18th international scientific conference "EcoBalt 2013", October 25-27, Vilnius, Lithuania,* 32;

14. **Šemčuk S.**, Lujanienė G., Tautkus S., Suchockaja D., 2013. Synthesis and application of graphene oxide for radionuclides removal from contaminated solution. *18th international scientific conference "EcoBalt 2013", October 25-27, Vilnius, Lithuania,* 31.

1. LITERATURE REVIEW

1.1. Materials for nanocomposite synthesis for radionuclides removal

The rapid industrial development, energy needs and, on the other hand, the high requirements of the environmental protection resulted in the development of new technologies based on the efficient and environmentally friendly materials. Graphene and related carbon materials such as graphene oxide, reduced GO and various GO based nanocomposites have attracted great attention since 2004, when the specific properties of graphene were discovered (Novoselov et al., 2004). The GO have a large surface area and a variety of oxygen-containing groups: hydroxyl (–OH), epoxy (C–O–C), carboxyl (–COOH) and carbonyl (–C=O). This makes it capable to sorb metals and radionuclide through coordination and electrostatic interaction. It also expands the use of GO as a precursor of graphene and a substrate for various chemical modifications (Park & Ruoff, 2009; Soldano et al., 2010; Dreyer et al., 2010; Singh et al., 2011). Their unique properties and a wide range of physical and engineering applications in various fields as well as their high potential for the efficient removal of various pollutants including the most toxic long-lived radionuclides from contaminated solutions made them the most promising materials of the 21st century (Mauter et al., 2008; Zhu et al., 2010; Ivanovskii et al., 2012).

1.1.1. Properties of graphene, synthesis methods and application features

One of the most plentiful elements in nature is carbon. It exists in many different structures which are called carbon allotropes. The general and the famous structures are graphite and diamond. The graphite structure is three-dimensional (3D) and consists of flat layers connected with each other perpendicularly. The layers consist of planar hexagonal structures of a carbon network of sp^2-hybridized carbon atoms. The one single layer of the graphite is called a graphene. The distance between these layers is 0.355 nm and the length of the strong covalent σ-type bond C-C in the layer is 0.142 nm (Soldano et al., 2010). The p orbitalis delocalized and π-type bonds extend perpendicular to the layers. The attractions between the layers are carried with weak Van der Waals forces. Mainly, the investigations on graphene were not performed widely until prof. A.K. Geim and prof. K.S. Novoselov in 2004 successfully observed a graphene monolayer. They used the Scotch-tape

technique to divide layers by breaking the Van der Waals forces between multilayer structure of graphite (Geim et al., 2007). It has been realized that graphene provides the excellent and unique physical and chemical properties such as two-dimensional (2D) atomically thin crystal, transparency (B98 %), strongest materials ever measured (200 times of steel), stiffest known materials (two times of diamond), most stretchable crystal (elastic up to 20 %), superfast charge mobility (200 times of silicon), and high thermal conductivity (two times of diamond), large specific surface area and etc. It is condensed matter analogue of (2+1)-dimensional quantum electrodynamics and can be used for a modeling. This phenomenon led the graphene to be the material of choice for numerous researchers in broad fields. In 2010, Greim and Novoselov shared the Nobel Prize in Physics for the discovery of graphene.

The production of monolayer graphene is a very difficult task, despite its simple structure. The graphene can be synthesized by five major techniques: (1) mechanical exfoliation, (2) epitaxial growth, (3) chemical vapor deposition (CVD), (4) organic synthesis and (5) chemical exfoliation methods (Byung et al., 2017). Comparisons of these methods are presented in table 1.1.

Table 1.1. Comparison of various graphene synthesis methods (Byung et al., 2017)

Method	**Advantages**	**Disadvantages**
Mechanical cleavage	High-quality graphene	Not scalable
Epitaxial growth	High-quality graphene	Discontinuous
Chemical vapor deposition	High-quality and large area	High cost and complex transfer
Bottom-up synthesis	Potentially suitable for mass production	Many defects
Chemical exfoliation and its reduction	Low cost and suitable for mass production	Many defects

One-layer graphene and bilayer graphene have simple electronic spectra. They are zero-gap semiconductors with one type of electron and one type of hole. However, the spectra of graphene containing more than two layers become too complicated. Considering all these features, it is easy to distinguish single-, double- and few- ($3 \leq 10$) layers graphene as three different types of 2D crystals “graphenes” (Shan et al., 2009).

The screening length in graphite is less than two layers thick and it is about 5 Å. That's why it is necessary to differentiate the surface and the bulk even for films as thin as five layers. Concentrated graphene can be isolated by chemical exfoliation of intercalating bulk graphite which causes the separation of graphene planes by layers of intervening atoms or molecules. This can result the formation of new 3D materials. Moreover, for some needs, large molecules can be inserted between atomic planes for greater separation. Such compounds can be considered as isolated graphene layers embedded in a 3D matrix. In addition, by changing the concentrations of interacting molecules in a chemical reaction, it is possible to obtain sludge consisting of restacked and scrolled graphene sheets (Dresselhaus et al., 2002). On the other hand, this method has an uncontrollable character without permanent result, which consequencesly is not attractive enough for the researchers.

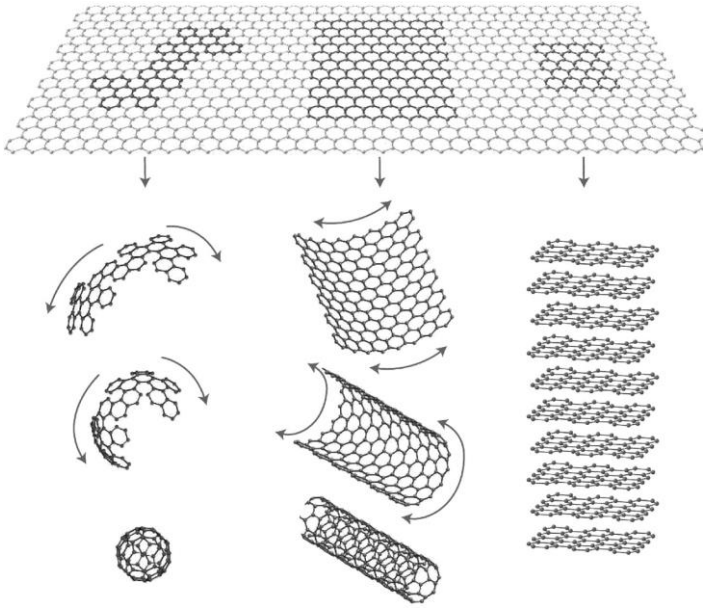

Fig. 1.1. Scheme showing graphene can be wrapped to 0D fullerenes, wrapped to form 1D carbon nanotubes or stacked to form 3D graphite (Geim, et al., 2007).

Graphene has wide potential applications due to its excellent mechanical, electrical, thermal, and optical properties and its large surface-to-weight ratio. The remarkable properties of graphene reported in the literature are as follows: mobility of charge carriers 200000 $cm^2 V^{-1} s^{-1}$, fracture strength ~ 125 GPa, surface area ~ 2630 $m^2 g^{-1}$ and thermal conductivity ~ 5000 $W m^{-1} K^{-1}$ (Soldano et al., 2010). Graphene has extended π-π

conjugation which results the exceptional optical, thermal, electrical properties and transport phenomena, such as the quantum Hall effect.

During the synthesis of graphene, it is possible that occur a surface defects, which lead to surface-active functional moieties. It can be a quioninic, C=C or even such reactive groups as carboxyl or ketonic which can easily bind covalently with bimolecular. Also, it can be used for further modifications for various biosensing applications. In addition, it is believed that chemically modified graphene and graphene are promising candidates for energy storage materials, polymer composites, paper-like materials, liquid crystal devices and mechanical resonators (Singh et al., 2011).

The term graphene was recommended by the IUPAC (International Union of Pure and Applied Chemistry) commission to replace the existing graphite layers term that was irrelevant in the single-carbon-layer structure research because a 3D stacking structure is identified as graphite. As a result, these days graphene refers to a 2D monolayer of carbon atoms and is considered as the basic building block of graphitic materials such as fullerene, carbon nanotube, and graphite (Kumar et al., 2014).

1.1.2. Comparison of methods for the synthesis of graphene oxide

Table 1.2. Synthetic methods can be used to synthesize GO.

Method	Used oxidant	Reaction media	C/O ratio	Raman spectral I_D/I_G ratio	Notes
Staudenmaier	$KClO_3$	HNO_3 + H_2SO_4	1.17	0.89	
Brodie	$KClO_3$	Fuming HNO3	-	-	$KClO_3$ added stepwise than in a single bolus
Hofmann	$KClO_3$	Non-fuming HNO_3	1.15	0.87	
Hummers	$KMnO_4$ + $NaNO_3$	Conc. H_2SO_4	0.84	0.87	Modifications can eliminate the need for $NaNO_3$
Tour	$KMnO_4$	H_3PO_4 + H_2SO_4	0.74	0.85	

In 1958, Hummers reported a method of preparing graphene oxide, which readily forms a stable colloidal suspension in water (Hummers et al., 1958). This suspension can be used for further production of single-layer graphene oxide by ultrasonic treatment. There are published many of studies on the synthetic methods of GO production, such as Brodie, Staudenmaier, Hummers, modified Hummers and Tour, listed in Table 1.2.

Each method has its own pluses and minuses, and the resulting GO has a different degree of oxidation. Also, the synthesis method depends on the properties and structure of GO.

- *Brodie method*. In 19th century a British chemist B.C. Brodie first time synthesized a graphene oxide. About 150 years ago he treated graphite repeatedly with potassium chlorate ($KClO_3$) and fuming nitric acid (HNO_3) (Brodie 1859).
- *Staudenmaier method.* Staudenmaier tried to improve previous Brodie method by using the concentrated sulfuric acid (H_2SO_4) to increase the acidity of the mixture. Another modification was the addition of more potassium chlorate ($KClO_3$) solution into the reaction mixture. As a result, he obtained a highly oxidized GO in a single batch reaction, thus reducing the experimental procedure. However, this method is hazardous and time-consuming. This method is rarely used for GO production (Staudenmaier et al., 1898).
- *Hummers method.* Hummers and Offeman in 1958 used a mixture of sodium nitrate ($NaNO_3$), potassium permanganate ($KMnO_4$) and concentrated sulfuric acid (H_2SO_4) for producing GO. The mixture was maintained below 45 ºC for about 2 hours for the oxidation of graphite. As a result, they synthesized a highly oxidized graphene (Hummers & Offeman, 1958). Despite the benefits of this method, it was not perfect enough because of incomplete oxidation of graphene. Thus, researchers tried to improve it and in 1999 Kovtyukhova introduced modified Hummers method, that led to obtain higher degree of oxidation. In this method, graphite was pretreated with a mixture of concentrated H_2SO_4, $K_2S_2O_8$, and P_2O_5 at 80 ºC for several hours. The mixture was filtered, rinsed, and dried before the Hummers method (Kovtyukhova et al., 1999). Usually, this method produces 1 nm thickness GO monolayers with surface dimensions from some nanometers to a few micrometers. Comparing with the Brodie method, the degree of oxidation of GO is improved and the chemical composition of product is about C:O:H =

4:2.95:2.5. In addition, to ensure high-quality of the product few purification steps are required.

- *Tour method.* In 2010 the Tour group proposed a better method for the synthesis of GO. The main difference from other methods was a usage of phosphoric acid instead of sodium nitride which was the source of toxic gases during the synthesis. The GO was synthesized using a $KMnO_4$ in a mixture of acids (H_2SO_4:H_3PO_4 in ratio 9:1). As a result, they produced high oxidized GO which had a surface with less defects comparing with GO prepared using the previous methods. (Marcano et al., 2010).

1.1.3. Properties of graphene oxide

The graphene oxide is a compound of carbon, oxygen and hydrogen in variable ratios, which can be obtained by treating graphite with strong oxidizers. The maximum oxidized graphene has a yellow color. The C:O ratio in this compound is between 2.1 and 2.9, and this keeps the layer structure of graphite but with irregular and larger spacing. In figure 1.2. the chemical structure of graphene oxide is shown.

Different synthesis methods and degree of oxidation depend on the properties and structure of graphene oxide. The synthesized GO usually retains the structure of the layer of the original graphite, but the interlayer distance is approximately twice as large as in graphite. Besides oxygen containing groups, other functional groups experimentally found are: carbonyl (=CO), phenol, hydroxyl (–OH), for graphite oxides prepared using sulphuric acid (e.g. Hummers method) also some impurity of sulphur is often found, for example in a form of organo-sulfate groups. The detailed structure of GO is still not studied enough because of strong disorder and irregular packing of the layers. The thickness of GO layers is about 1.1 ± 0.2 nm (Schniepp et al., 2006). Scanning tunneling microscopy shows that the edges of each layer are terminated with carboxyl and carbonyl groups. Furthermore, oxygen atoms on the layers can arrange in a rectangular pattern.

Graphene oxide is an insulator, almost a semiconductor, but it is hydrophilic and easily hydrated in water. This leads to the increasement of the inter-planar distance with additional water incorporation into interlayer space. 2-3 water monolayers can be placed between layers to reach the maximal hydration state of graphene oxide in liquid water. Complete removal of water from the structure is a difficult task because of degradation and partial decomposition of the material during the heating at 60 – 80°C. GO also can

incorporate with polar solvents, but intercalation is significantly different comparing with water. The distance between GO layers usually increases proportionally to the size of solvent molecule (Gómez-Navarro et al., 2007).

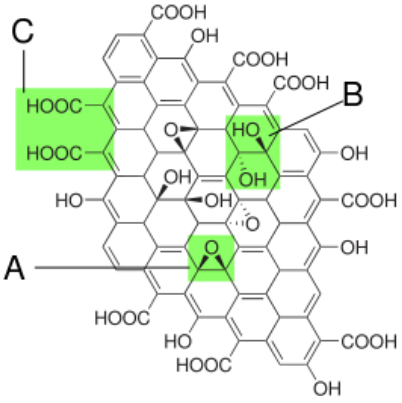

Fig. 1.2. The chemical structure of graphene oxide containing A – epoxy, B – hydroxy and C – carboxyl groups (Hea et al., 1998).

Since the last decade, graphene began to be explored as a membrane because of its special properties. The ability to create selective nonporous, large area sheet of one atom thick, which have a strong but elastic crystal structure are the main demands for membrane applications. Despite the fact that for graphene and its derivatives (for example, graphene oxide, functionalized graphene) there are many obstacles for real applications in membranes, graphene will continue to develop rapidly in membrane applications, in particular such as gas-liquid separation (Byung et al., 2017). In addition, it is believed that graphene-based nanocomposites are suitable for adsorptive treatment of contaminated water (Wang et al., 2013 a; Wang et al., 2013 b).

Another use of GO is like a membrane. According to Josia et al., membrane is considered as a barrier with an ability to allow the passage of certain species while blocks other depending on characteristics of the membrane and species to be filtered. Membrane technology is a rapidly growing research area with several real time applications such as desalination and water purification. Scientists and engineers have been working towards the development of this technology for a more cost-effective and a precise membrane. Traditionally, membranes have been classified in to two types and they are polymeric and inorganic membranes (Joshia et al., 2015).

Recently, graphene oxide has emerged as excellent membrane material. In 2012 Nair et al. demonstrated that GO membrane allows unimpeded permeation of water where as it blocks everything else in the vapor form. However, their work does not rule out the joint propagation of organic molecules dissolved in water through GO membrane. The ease in making atomically thin GO layers in the form of membrane provides an edge over other membranes for their practical applications. Graphene, in general, does not allow anything to pass through. Graphene oxide is continuously demonstrating its excellent membrane characteristics and offer huge potential for real applications (Nair et al., 2012).

Graphite oxide has attracted much interest recently as a possible route for the large-scale production and manipulation of graphene, a material with extraordinary electronic properties. Graphene oxide was applied to the removal of Co^{2+} and Cd^{2+} ions (Zhao et al., 2011), Cu^{2+} (Wu et al., 2013; Sitko et al., 2013) with sorption capacities from 106.3 mg g^{-1} to 68.2 mg g^{-1}, while maximum sorption capacities (Q_{max}) as mentioned by Sun et al., 2012 and Jia & Lu, 2014 for Pb^{2+} were found to be up to 1119 mg g^{-1}. It was believed that decrease of pH after sorption was is an indication of ion exchange and complexation on surface of sorbent as main adsorption mechanisms. The poor attention was paid for the effect of pH on sorption of metals and radionuclide to GO. The effect of final pH in solution on adsorption of Cu^{2+} was reported only in one publication (Wu et al., 2013). Treatment of contaminated water is one of the most important tasks of environmental protection. Various kinds of sorbents were applied to solve these problems (Hua et al., 2012., Lujanienė et al., 2009); however, they do not always meet the high standards of environmental protection.

1.2. Modifiers increasing the ability of GO to sorb contaminants

Various kinds of graphene oxide based composites were used for treatment of contaminated solutions, e.g., the sulfonated magnetic GO composite and magnetic mn-doped Fe(III) oxide nanoparticle implanted graphene for Cu^{2+} (Q_{max} – 18.3 mg g^{-1} - 129.7 mg g^{-1}) and for Pb^{2+} (Q_{max} – 274.7 mg g^{-1} - 673 mg g^{-1}) as well as the magnetic GO composite for Cu^{2+} (the obtained Q_{max} of 59.44 mg g^{-1}) and for Pb^{2+} with Q_{max} of 151.17 mg g^{-1} (Li et al., 2012; Hu et al., 2013; Nandi et al., 2013; Kumar et al., 2014 ; Zhang et al., 2014 ; Hur et al., 2015). GO based sorbents were applied to remove $Sr^{2+}$and Cs^{+} ions from wastewater. The higher adsorption was observed at pH > 6.0 and Q_{max} was found to be 14.706 and 9.259 mg g^{-1} for $Sr^{2+}$and Cs^{+},

respectively. It was reported that the adsorption kinetics of Sr^{2+} and Cs^{+} on magnetic GO satisfactorily fitted to the pseudo-second-order kinetic model. Authors showed that magnetic GO composites could be used for the immobilization and pre-concentration of radionuclides from aqueous solutions in environmental cleanup (Li et al., 2015). The synthesis of the reduced graphene oxide (r-GO) dendrite nanocomposite has been reported by Roy et al. The r-GO sheet was conjugated with silane group modified magnetic nanoparticles which further reacted with a new r-GO sheet, resulting in the formation of r-GO dendrite. It is believed that the composite can be useful for inhibition of the bacterial growth and selective magnetic separation of europium ions (Roy et al., 2015).

1.2.1. Chitosan

Chitosan is one of most plentiful and low-cost biopolymers in the world. The chemical structure of chitosan or poly-(1→4)-2-amino-2-deoxy-b-d-glucose is presented below in Fig. 1.3. It can be used as an adsorbent for removing pollutants from wastewater due to its high amino and hydroxyl functional group content (Kavitha et al., 2011, Liu et al., 2012).

This biopolymer has linear and heterogeneous structure with high molecular weight. Chitosan is nontoxic and cationic, biocompatible and biodegradable polysaccharide. Chitosan is produced from chitin. During the alkaline deacetylation process of chitin (Fig 1.4), the acetyl groups are hydrolyzed and converted to free amine groups (Rinaudo 2006). Chitin can be extracted from chitin shells of sea creatures such as lobster, crab and other crustaceans (Muzzarelli et al., 1994).

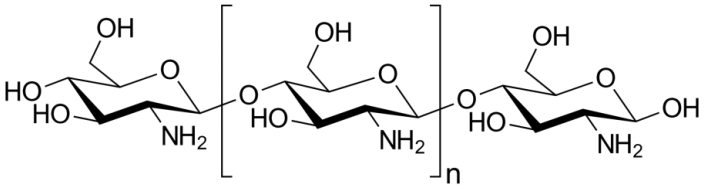

Fig. 1.3. The chemical structure of chitosan.

The ratio of deacetylated to acetylated units shows the degree of deacetylation (DD) of chitin. It is an important parameter for characterization of chitosan because it influences the sorption capacity of the chitosan (Jana et al., 2013). Another important property is crystallinity, because it also affects

the adsorption capacity of chitosan (Guibal, 2004). Chitosan is insoluble in water, alkaline solutions and organic solvents, but soluble in acidic solutions.

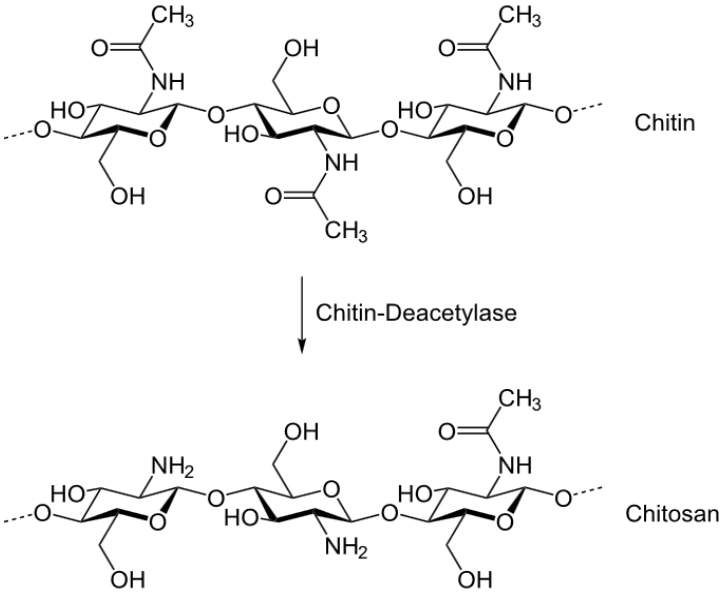

Fig. 1.4. Production of chitosan by deacetylation process of chitin

Chitosan has affinity to sorb pollutions such as heavy metals due to availability of functional groups on it (Ren et al., 2013). On the other hand, low surface area and low mechanical strength limits the sorption performance of it. This led to modification of chitosan or use it to modify other materials to achieve the best sorption of impurities. For example, chitosan was modified with Fe^0 (Geng et al., 2009), $MnFe_2O_4$ (Ren et al., 2012) and Fe_3O_4 (Fan et al., 2011), or even further modification of magnetic chitosan with other substrate such as SiO_2 (Egodawatte et al., 2015), cellulose (Beyki et al., 2014), carbon nanotubes (Lu et al., 2017), etc.

Those composites have been applied for effective adsorption of target metal ions with different adsorption capacity, Fe_3O_4/mesoporous silica (Q_{max} – 36.92 mg g^{-1}) and Fe_3O_4/mesoporous silica-NH_2 (Q_{max} – 108.16 mg g^{-1}) used for Cr^{3+} (Egodawatte et al., 2015), Fe_3O_4/cellulose xanthate(1) (Q_{max} – 166.0 mg g^{-1}) and Fe_3O_4/cellulose xanthate(2) (Q_{max} – 15.62 mg g^{-1}) used for Ag^+ (Beyki et al., 2014), magnetic thiourea-chitosan imprinted Ag+ (Q_{max} – 531.79 mg g^{-1}) used for Ag^+ (Fan et al., 2011) and magnetic iron oxide nanoparticle-multiwalled carbon nanotube (Q_{max} – 22.22 mg g^{-1}) used for Cr^{6+} (Lu et al., 2017).

1.2.2. Prussian blue

Prussian blue (PB) is a dark-blue pigment, has the formula $Fe_7(CN)_{18}$, which is generally synthesized by reaction of potassium (or sodium) hexacyanoferrate with iron (III) chloride giving different compounds with different solubility properties. In the presence of an excess of iron (III) chloride, PB turns from a soluble/colloidal form ($KFe[Fe(CN)_6]$) to an insoluble form generally described as $Fe_4[Fe(CN)_6]_3$ (Faustino et al., 2008). It was discovered approximately 300 years ago and is well documented in the works of Berlin and Kraft (Kraft A. 2008). Prussian blue and its analogs (other metal hexacyano compounds) are used in the electromagnetic, biomedical, biochemical, and electrochemical fields (Johansson et al., 2005). Prussian blue (PB) is an ion-exchanger that is well known for its affinity for some light earth metal ions such as cesium(I) or rubidium(I) (Faustino et al., 2008). For medical applications, Prussian blue is known as an effective radio toxin remover which is administered orally under the form of tablets/capsules for radioactive ^{137}Cs absorption with dosage up to 10 g day^{-1} (Thompson D.F., et al. 2001). The Fukushima reactor accident has accelerated the research on radioactive decontamination of Cs using PB (Sasaki & Tanaka, 2012). Hee-Man et al., (2016) applied Prussian blue-functionalized magnetic nanoclusters for removal of Cs from water with further rapid magnetic separation.

1.2.3. Magnetite

Nanocomposites possessing magnetic properties are especially useful since they can be easily eliminated from the solutions after the treatment procedures. Iron oxide nanoparticles are widely used for biomedical applications such as drug delivery, cancer therapy, separation of biochemical products, etc. The surface modification of Fe_3O_4 (magnetite) was reported with materials such as polymeric liposome, polyvinyl alcohol, SiO_2, poly vinyl pyrrolidone (PVP), TiO_2, gold, silver and a variety of other surface modifiers (Arun et al., 2013). Magnetic nanoparticles functionalized with groups that can adsorb contaminants, such as heavy metals, have been widely examined for the treatment of contaminated water because they can be magnetically separated from a solution simply by application of an external magnet. Recently, magnetic nanoparticles coated with Prussian blue (PB), which is a metal-ferrocyanide complex with a strong selectivity for binding inactive Cs, were used to treat ^{137}Cs contaminated water and subsequently

separated via the application of an external magnet (Ambashta & Sillanpaa, 2010).

1.3. Factors affecting the sorption parameters

The variety of techniques are used for removal of radionuclides from aqueous solutions for example ion exchange, membrane, precipitation, bio-remediation, adsorption and solvent extraction (Metwally et al., 2016). The adsorption technique was chosen for this study because it is widely used to eliminate of radionuclides from large volumes of aqueous solutions due to its simple operation and low-cost process. It should be noticed that sorption parameters such as contact time, solution pH, temperature and dosage of adsorbent have significant impacts on the adsorption property of nanocomposites for target ions. Moreover, the influence of co-existing ions should also be considered in the adsorption systems. Usually, optimizing process variables of target ion removal are carried out mainly by one or few factors, for example time and cost or sorption capacity (Zhang et al., 2016).

1.3.1. Effect of pH

One of the significant variables of the sorption process is solution pH. It affects the speciation of target ion, ionization degree and also, the sorbent or its surface characteristics. (Zhang et al., 2016). Magnetic graphene oxide sorbents were applied to remove $Sr^{2+}$and Cs^{+} ions from wastewater. The higher adsorption was observed at pH > 6.0 and Q_{max} was found to be 14.706 and 9.259 mg g^{-1} for $Sr^{2+}$and Cs^{+}, respectively. Authors showed that magnetic GO composites could be used for the immobilization and pre-concentration of radionuclides from aqueous solutions in environmental cleanup (Li et al., 2015). Dragan used a chitosan/poly (vinyl amine) composite beads for Cu^{2+} sorption in pH rage of 2.0 – 5.5 and results showed that adsorption capacity of Cu^{2+} increased when initial pH was increased from 2.0 to 4.5, but with a further increasement of pH to 5.5 it decreased (Dragan et al., 2014). Yakun et al. reported that the sorption efficiency of Pb (II) and Hg (II) on the magnetic $CoFe_2O_4$rGO composite varied depending on pH – the sorption decreases at low (pH < 5.0) was attributed to the repulsive forces while an increase in the adsorption capacity at pH >4 was explained by the electrostatic attraction and monolayer uniform adsorptions. Therefore, it is important that the produced nanosorbent could efficiently sorb target ions or radionuclides at a wide range of pH values (Yakun et al., 2014).

1.3.2. Effect of temperature

Another important parameter for the adsorption of target ion using the adsorbents is temperature. It affects the solid/liquid interfaces, the mobility of target ions and the property of used sorbents. The increasement of temperature usually increases effects mentioned before. On the other hand, increasement of temperature can induct the desorption process from sorbents (Zhang et al., 2016). That's why for this study, normal conditions were chosen, the initial temperature of the solutions was 20±2 °C.

1.3.3. Effect of co-existing ions

The presence of co-existing ions (such as K^+, $Na^{+,}$ Cl^-, NO^{3-}, SO_4^{2-}, PO_4^{3-} and other metal cations) in solutions will lead to competitive adsorption which could affect the removal efficiency of target ions onto sorbent. For example, Mishra et al. (2013) revealed that NaCl and Na_2SO_4 had significant effects on the adsorption capacities of Cd (II) by Ch-g-CD at pH 8.5, and they reported that removal of cadmium decreased from 36.91 to 18.34 mg g^{-1} and from 34.26 to 14.88 mg g^{-1} with an increase in concentration of NaCl and Na_2SO_4 from 0.01 to 1.0 M, respectively.

1.3.4. Sorption capacity of sorbents

Generally, application of nanocomposites shows wide variations in obtained Q_{max} values. The highest reported Q_{max} values determined for Cs (I), Sr (II), Eu (III) and U (VI) are 142.8 mg/g, 1.68 mmol/g, 1.65 mmol/L and 1.03 mmol/g, respectively. Sorption mechanisms have been attributed to various processes such as electrostatic attraction, ion exchange, chemisorption, inner-sphere or outer- surface complexation and varied depending on the studied nuclide and sorbent involved (Xiangxue et al., 2015; Wenqin et al., 2013; Seung-Mok et al., 2012). Sorption of U (VI) ions by nZVI/rGO composites was mainly ascribed to the surface complexation, after spontaneous adsorption of U (VI) on rGO and the reduction of U (VI) to U (IV) (Sun et al., 2014).

1.4. Clays in radioactive waste disposal

The geological repositories are used for isolation of nuclear waste and their processed forms from the biosphere. Such safe and effective disposal sites usually consist of technical, geotechnical and geological barriers (Norrfors et al., 2016). Containers with radioactive wastes are surrounded by the geotechnical barrier which is composed of natural clay minerals. The main purpose of multi-barrier concept is to retard radionuclide migration towards the biosphere if the container would leak (Kumar et al., 2013). Therefore, it is very important to estimate sorption and desorption parameters of radionuclides for materials used in engineered barriers for better analysis and understanding of many processes that can affect safety of low and intermediate level radioactive waste disposal sites (Lujanienė et al., 2006).

Natural clays have a variety of reactive minerals, such as almandine, grossular, goethite sillimanite, pyrite, hematite, andalusite, magnetite, siderite, smectite, kyanite, pumpellyite, spodumene, lepidolite, illite, sodalite, hydroxyapophyllite, stilbite, heulandites and other (Xu & van Deventer, 2000). Clay minerals are most efficient for fast sorption of pollutants due to their high sorption capacities and they possess low permeability. Moreover, they are self-healing and self-sealing. In addition, they can form the inner- or outer-sphere surface complexes. Such properties retard pollutant migration and are profitable for the restriction of potentially hazardous materials (Tournassat et al., 2013, Grangeon et al., 2015). There are published many studies on natural clay properties and its use for retardation of pollutants. For example, Norrfors et al. used clay and separated montmorillonite colloids (clay mineral) for ^{232}Th, ^{99}Tc, ^{233}U, ^{237}Np and ^{242}Pu radionuclide removal. During the experiment Th (IV) and Pu (IV) were adsorbed on the larger montmorillonite particles (Norrfors et al. 2016). Hoving et al. used clays for studying of redox reactions with Fe-containing minerals in clay-rich sediments. Pyrite, siderite, smectite and illite were used separately in the research (Hoving et al., 2017). In this study, natural clay samples from the industrial exploitation Šaltiškiai site located at the North Lithuania were carefully characterized and applied to study changes in the oxidation state of plutonium and its sorption behavior in the natural clay-groundwater systems.

Plutonium is one of the most toxic elements that has been released into the environment. The prediction of its behavior and repartition is a complicated task, which needs an attention of researchers for better its understanding. Plutonium under environmental conditions can exist in five different oxidation states: Pu (III) represented by the ion Pu^{3+}, Pu (IV) - Pu^{4+},

Pu (V) - PuO_2^+, Pu (VI) - PuO_2^{2+} and Pu (VII) – PuO_5^{3-}, the most common of them are Pu (IV) and Pu (V) (Choppin 2007). It means that the speciation, solubility and transport properties of plutonium in the environment can vary during its hydrolysis, complexation and redox reactions (Powell et al., 2005). Moreover, the study of sorption behavior of Pu in natural clays is helpful for the selection of suitable clay minerals for conservation of nuclear wastes and for better prediction purposes (Lujanienė et al., 2015).

2. MATERIALS AND METHODS

2.1. Synthesis of sorbents

2.1.1. The synthesis of graphene oxide

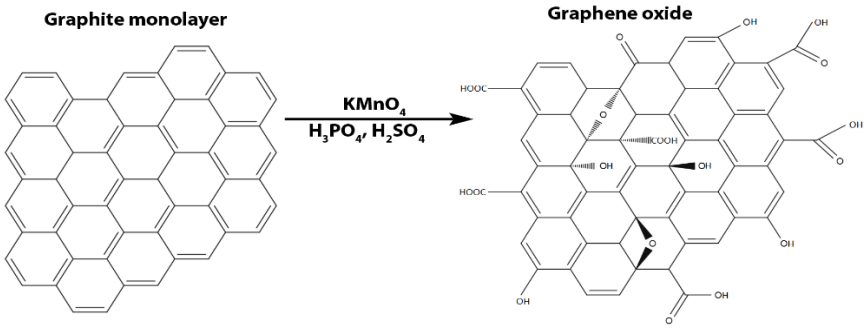

Fig. 2.1. Synthesis scheme of graphene oxide

After studying many methods described before of synthesis of GO, the modified Hummers' method was chosen. The graphite powder (<20 μm synthetic, Sigma Aldrich, Switzerland) was used for the synthesis of the graphene oxide (Hummers et al., 1958; Marcano et al., 2010). The powder was added to the mixture of H_2SO_4 and H_3PO_4 acids. Then slowly the $KMnO_4$ was gradually added with stirring into under controlled temperature. After careful mixing of all components, the solution was left under vigorous stirring for 24 hours at 50 ºC temperature. The reaction was stopped by adding the solution into the ice bath with H_2O_2 (30 wt. %). As a result, the solution turns yellow, which indicates a high level of oxidation. After all the resulting mixture was filtered and washed with Milli-Q water, acid solutions and alcohol, respectively, and then dried at 70 ºC under vacuum.

2.1.2. The synthesis of magnetic graphene oxide nanocomposite

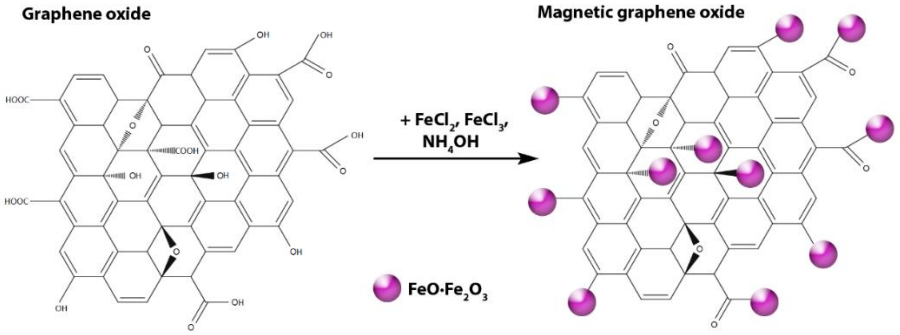

Fig. 2.2. Synthesis scheme of magnetic graphene oxide nanocomposite

The MGO nanocomposite was prepared by the co-precipitation reaction of Fe (II) and Fe (III) ions on the synthesized graphene oxide sheets (Prakash et al., 2012). Briefly, the aqueous suspension of GO was vigorously stirred under the N_2 atmosphere as well as $FeCl_3$ and $FeCl_2$ were added to the suspension of GO. Stirring of the mixture was continued at 80 ºC and NH_4OH was introduced into the reaction mixture. Then the hydrazine hydrate was added to ensure a complete reduction. The mixture was cooled and washed several times with Milli-Q water, using the magnet for separation. After that MGO was dried 24 hours at 60 °C temperature.

2.1.3. The synthesis of Prussian blue graphene oxide nanocomposite

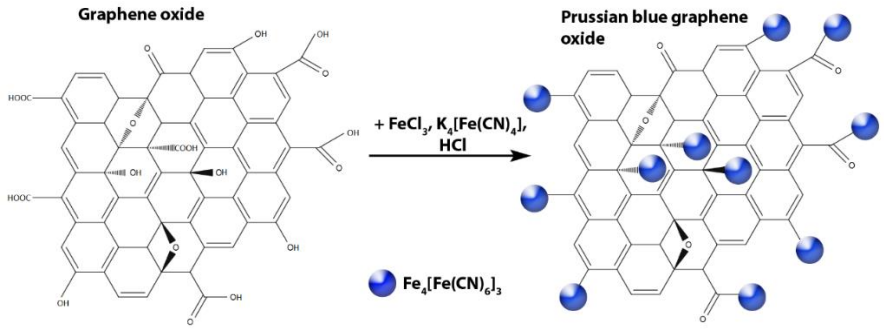

Fig. 2.3. Synthesis scheme of Prussian blue graphene oxide nanocomposite

Well dried graphene oxide was mixed with water and the solution is dispersed in an ultrasound bath. The ferrous chloride ($FeCl_3$) was added into a well stirred solution. After two hours of intense mixing the potassium iron

cyanide solution ($K_4[Fe(CN)_6]$) was slowly introduced. The solution is left on a magnetic stirrer for another hour and then acidified with 10 % acid. The resulting Prussian blue graphene oxide composite is washed with Milli-Q water to pH = 7 and then left in the drying oven at 60 °C for one day (Xia-Wang et al., 2010).

2.1.4. The synthesis of magnetic Prussian blue graphene oxide nanocomposite

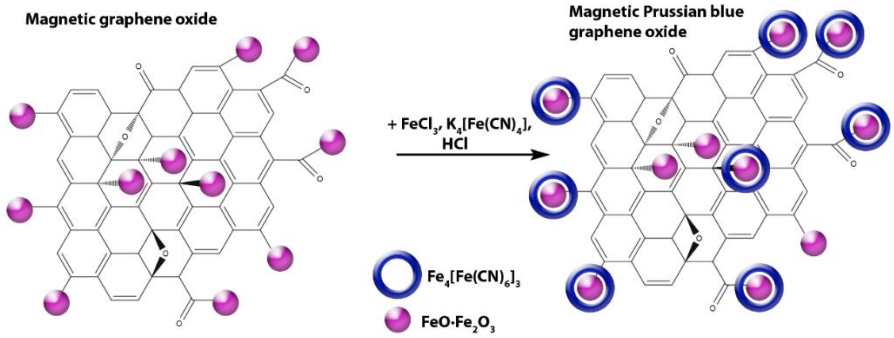

Fig. 2.4. Synthesis scheme of magnetic Prussian blue graphene oxide nanocomposite

The magnetic Prussian blue graphene oxide (MPBGO) sorbent was synthesized using the prepared magnetic graphene oxide composite. As it was mentioned above, the aqueous suspension of GO was mixed together with $FeCl_3$ and $FeCl_2$. Then the NH_4OH and N_2H_4 were introduced into the reaction mixture. After washing process with Milli-Q water using the magnet for separation, the resulting brown precipitate was re-dispersed in water. Then aqueous solution of $FeCl_3$ under stirring was added to the precipitate suspension, and aqueous solution of $K_4[Fe(CN)_6]$ was slowly introduced into the mixture drop by drop. The stirring of the mixture was continued for 1 hour. The obtained precipitate was washed with water and dried at 50 ºC (Hongjun et al., 2014).

2.1.5. The synthesis of chitosan graphene oxide nanocomposite

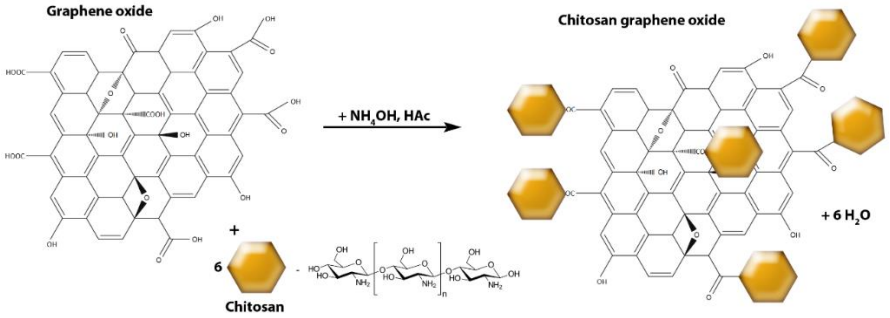

Fig. 2.5. Synthesis scheme of chitosan graphene oxide nanocomposite

The synthesis of chitosan graphene oxide nanocomposite was carried by preparing the hydro gel as mentioned in Heng Zhao et al., 2015 paper. The aqueous dispersion of GO (2.0 mg/mL) prepared via ultrasonic bath was mixed with 120 mL of CS (30.0 mg/mL, prepared in 1% acetic acid (HAc) solution) in a glass. The hydro gel was sonicated for 10 min, in order to obtain a homogeneous gelation state, after that precipitated using sodium hydroxide (NaOH 1 M) ethanol mixture. The prepared nanocomposite was washed several times using the ethanol and acetonitrile. Before using the CSGO in sorption experiments, it was washed with water until neutral pH.

2.2. Characterization of synthesized nanocomposites

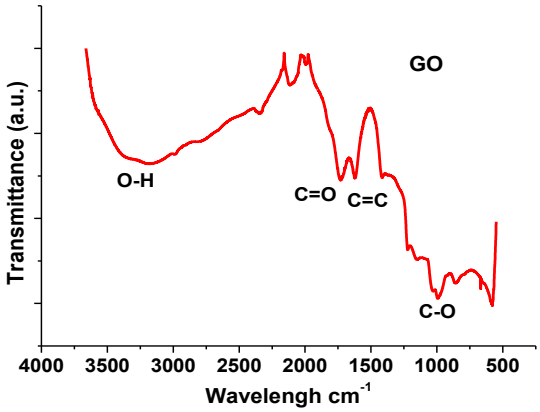

Fig. 2.6. FTIR spectra of synthesized graphene oxide

Researchers, for example Hareema Saleem (2018), Santosh Kumar (2014) use FTIR (Fourier Transform Infrared spectroscopy) spectra to provide information about the functional groups in a sample. Usually, it is need to confirm the qualitative synthesis of the composite. For analysis the tablet of 5 mm thickness is prepared using the mixture of dried graphene oxide and heated potassium bromide under 50 kPa pressure in a die. In figure 2.6, the FTIR spectra of graphene oxide is presented. The existence of O–H, C=O, C=C and C–H bonds given in the spectra make as sure that GO has been synthesized during oxidation of graphite. We can see the peaks of O-H (stretching vibrations), sp^3 C–H, C=O (stretching vibrations) and C=C (skeletal vibrations from unoxidized graphitic domain) C–O (epoxy group) bonds showed at 3394 cm^{-1}, 2920 cm^{-1}, 1723 cm^{-1}, 1619 cm^{-1} and 1080 cm^{-1} wavelengths. It is well established that GO contains various types of oxygen functional groups such as hydroxyl, carbonyl, alkenes and epoxy functional groups.

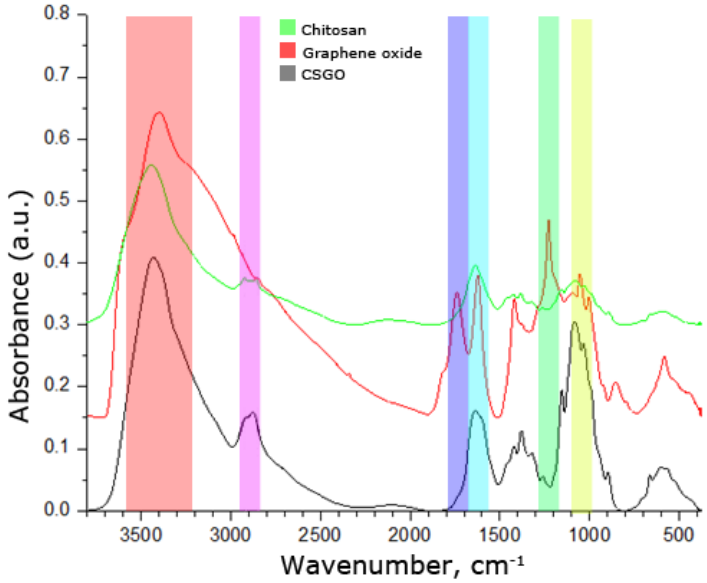

Fig. 2.7. FTIR spectra of (1) chitosan grapheme oxide nanocomposite, (2) graphene oxide and (3) chitosan

FTIR spectrum of graphene oxide is presented in figure 2.7 – 2. The typical peaks for oxygen containing groups on graphene oxide ─ O–H (~3400 cm^{-1}), C=O (~ 1740 cm^{-1}), C=C (~ 1610 cm^{-1}), O–H (~ 1420 cm^{-1}), C–O (~ 1230 cm^{-1}), C–OH and C–O–C (~ 1000 – 1100 cm^{-1}) ─ can be seen in the spectrum.

The typical peaks of O–H (~ 3450 cm^{-1}), C–H (~ 2900 cm^{-1}), N – H (~ 1620 cm^{-1}), C–OH (~ 1080 cm^{-1}) groups are characteristic of chitosan (Yan H. et al., 2016), while in the spectrum of CSGO (fig. 2.7. (1)) nanocomposite peaks in areas of ~ 1740 cm^{-1} (C=O) and ~ 1230 cm^{-1}(C–O) are usually not observed (Yi H., et al. 2013). The disappearance of these peaks is an indicative the chitosan-graphene oxide formation.

Chitosan FTIR spectra (Fig. 2.7. (3)) show functional group relationships: O–H (~ 3450 cm^{-1}), C–H (~ 2900 cm^{-1}), N–H (~ 1620 cm^{-1}), C–OH (~ 1080 cm^{-1}). Graphene oxide FTIR spectra shows the functional group relationships: O–H (~ 3400 cm^{-1}), C=O (~ 1740 cm^{-1}), C=C (~ 1610 cm^{-1}), O–H (~ 1420 cm^{-1}), C–O (~ 1230 cm^{-1}), C–OH and C–O–C (~ 1000 – 1100 cm^{-1}). Chitosan graphene oxide nanocomposite FTIR spectra are visible coincident peaks from both graphen oxide and chitosan spectra, except graphene oxide peaks at ~ 1740 cm^{-1} and ~ 1230 cm^{-1}. A ~ 1740 cm^{-1} peak represents aldehyde or ester C=O groups. A ~ 1230 cm^{-1} peak indicates a C–O connection near the double link. The disappearance of these groups during the reaction may indicate that the groups were involved in the chitosan joining reaction.

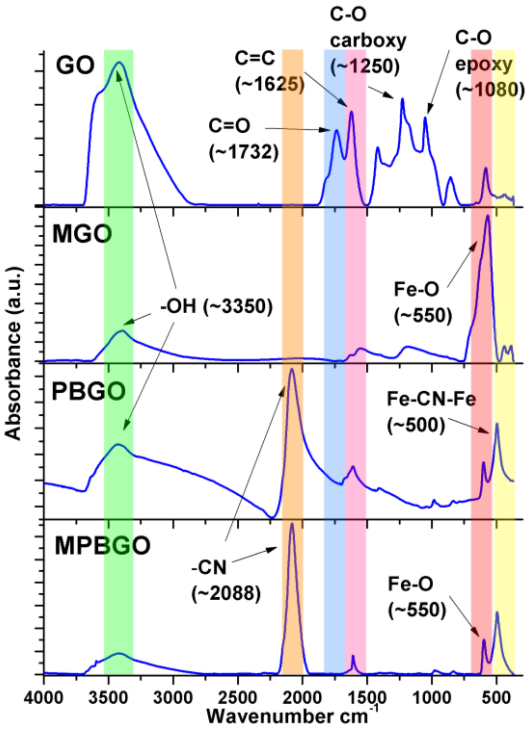

Fig. 2.8. FTIR spectra of graphene oxide and magnetic graphene oxide, Prussian blue graphene oxide, magnetic Prussian blue graphene oxide synthesized nanocomposites

The graphene oxide and its based nanocomposites FTIR spectra are presented in figure 2.8. In the spectrum of GO the peak at 1732 cm^{-1} characterizes the C=O bond. The peak at 3450 – 3300 cm^{-1} belongs to intra- and inter- molecular O–H vibrations. The peak at 1625 cm^{-1} is attributed to the aromatic C=C bond. Peaks at 1250 cm^{-1} and 1080 cm^{-1} are characteristic for carboxy and epoxy functional groups, respectively. The resulting GO FTIR spectrum coincides with the spectra provided by Si et al., 2008.

In the FTIR spectra of synthesized MGO and MPBGO nanocomposites the characteristic peaks of carboxyl groups disappeared: 1732 cm^{-1} and 1250 cm^{-1}. Characteristic peaks for iron oxide (Fe–O) bond vibrations appeared at 550 cm^{-1}. The corresponding peaks at 2088 cm^{-1} and 500 cm^{-1} were identified like the C–N and CN–Fe bonds vibrations belonging to the Prussian blue. Also, in the FTIR spectra of the Prussian blue graphite oxide nanocomposite, the characteristic peaks of the CN–Fe and C–N groups are visible, but there are no peaks at 1732 cm^{-1} and 1250 cm^{-1} again. The disappearance of these peaks proves that the carboxyl groups are involved in the graphene oxide modification reaction.

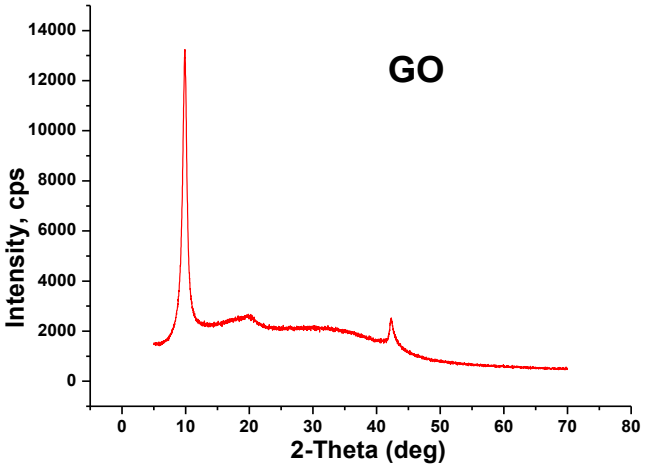

Fig. 2.9. The XRD spectrum of synthesized graphene oxide

Synthesized graphene oxide was characterized by X-Ray diffraction analysis. Its XRD spectrum is presented in fig. 2.9. The sample was pressed before testing. Diffractive region of graphene oxide is observed at $2\theta = 11°$. This peak shows the distances between the graphene layers when they are parallel to the surface of the diffractometer table. Peak size is proportional to the distance between planes. The increase of *d*-spacing is due to the intercalation of –OH functional groups between the layers of graphene. The

studies of pristine graphite, carried by Santosh Kumar et al., 2014, showed very intense peak at $2\theta = 26°$.

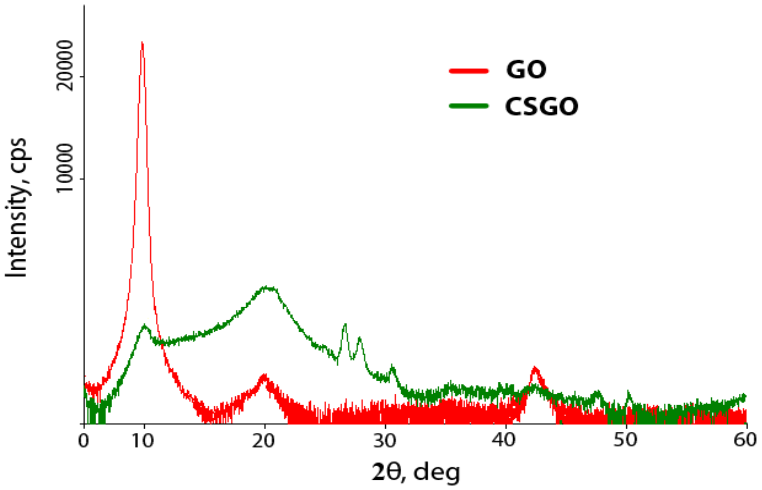

Fig. 2.10. The XRD spectrum of graphene oxide and chitosan graphene oxide nanocomposite

Pure chitosan films showed a characteristic peak at around $2\theta = 11°$ and sharp peak at $2\theta = 20°$ in figure 2.10. Studying the spectrum of synthesized CSGO nanocomposite, a small peak was observed at $2\theta = 11°$ and a weak wide peak at around $2\theta = 21$ °. The peak at $2\theta \cong 10°$ shows the distances between the graphene sheets when they are parallel to the surface of the diffractometer table. Peak size is proportional to the distance between planes. When comparing GO and graphite, the resulting distance ratio is 2.67:1. This shows that the gap between the graphene planes obtained in the resulting GO is 2.67 times that of graphite. This increase in distance is due to the interception (linking) of oxygen-containing groups (–OH, –O–) between graphs. Peaks at $2\theta \cong 20°$ show distances in hexagonal graphene planes. The peak is more intense when the graphene plane is located horizontally on the surface of the diffractometer table. Peaks at ~ 26-29° show the CSGO composite in crystalline impurities. Through the database, impurities are identified as quartz - sand. The samples are pressed before testing by X-ray diffraction analysis. The small functional groups (–OH, –O–) do not interfere with the spreading of the graphene leaves in parallel to each other, the intense peak is observed at ~ 10° and the non-intrusive peak at ~ 20°. When the large compounds (chitosan) attached to the graphene plates can no longer be positioned parallel to each other, an inert peak is obtained at ~ 10°.

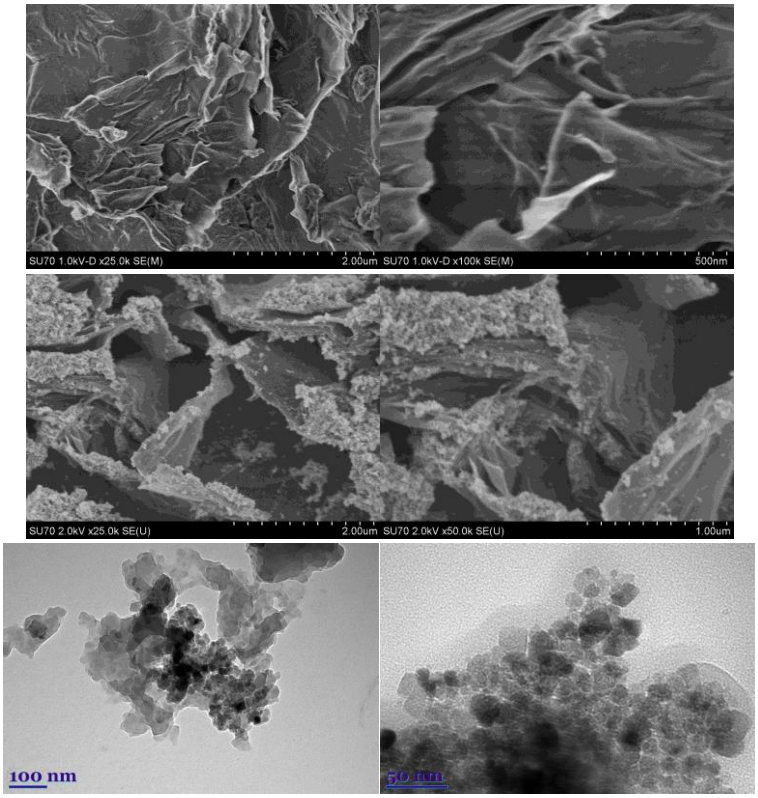

Fig. 2.11. SEM images of the synthesized graphene oxide, magnetic graphene oxide nanocomposite and TEM images of the chitosan graphene oxide nanocomposite

SEM and TEM images were taken to determine the surface morphology of the synthesized graphene oxide and it based nanocomposites, which are presented in fig. 2.11. As it can be seen in the SEM images of GO, the surface structure does not have the characteristic features of graphite. SEM images of MGO showed that magnetite particles appear on the GO surface, which again confirms that magnetite attaches on the surface of GO during the synthesis. On the TEM images of chitosan graphene oxide, we see a nanocomposite of two substances where the chitosan polymers are associated with graphene oxide.

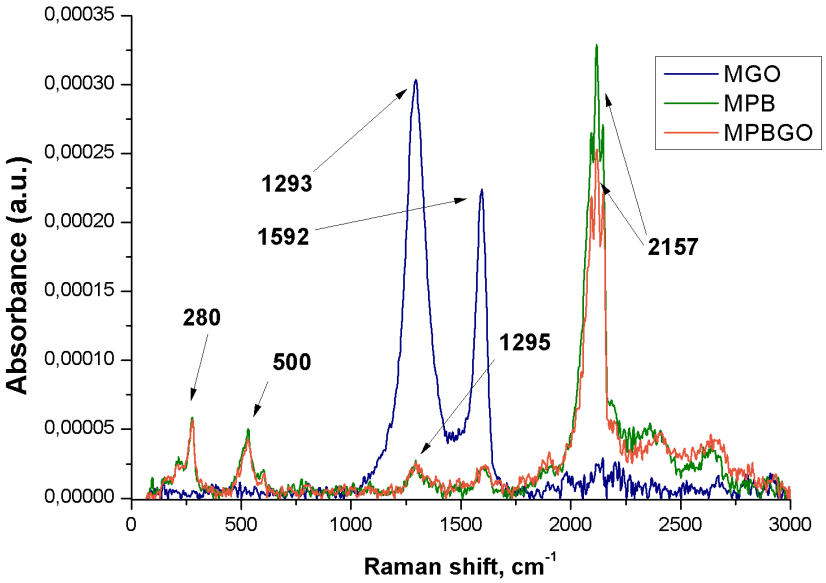

Fig. 2.12. The Raman spectrum of synthesized magnetic graphene oxide, magnetic Prussian blue and magnetic Prussian blue graphene oxide nanocomposites

The Raman spectrum of synthesized MGO, MPB and MPBGO composites are presented in figure 2.12. Two main bands of graphene oxide are demonstrated in the spectrum of MGO, the peak at ~ 1293 cm^{-1} and at ~ 1592 cm^{-1}. Typical peaks of Prussian blue were found at ~ 220 cm^{-1}, ~ 280 cm^{-1}, ~ 500 cm^{-1}, ~ 1300 cm^{-1} and ~ 2150 cm^{-1} in spectra of MPB and MPBGO. In spectra of magnetic Prussian blue graphene oxide composite there were no characteristic peaks for graphene oxide. This fact shows that Prussian blue particles can combine not only with the surface of magnetite, but also with active groups in the surface of graphene oxide sheets. This indicates the different structure of MPBGO synthesized composite as compared with that described in publication of Yang et al., 2014 where Prussian blue covered only magnetic particles.

2.3. Batch sorption experiments

For the study of the sorption of elements using synthesized nanocomposites the batch technique was chosen. For each experiment three sets were conducted. Sorption experiments were carried with the initial concentration of 50 – 700 mg L^{-1} of studied elements and 1 g · L^{-1} dosage

of sorbent. The WTW pH-electrode SenTix 41 was used to monitor the pH of solutions ranged from 1 to 9. The pH of suspensions was adjusted by adding 0.001 mol·L^{-1} HCl (or $HClO_4$ in experiments with Am and Pu) and NaOH. The measurements of pH in solutions were carried out before and after sorption. The centrifuge tubes were shaken for 48 h to achieve equilibrium until the pH remained stable over the desirable range (±0.1 pH units). ^{239}Pu (IV) and ^{241}Pu or ^{241}Am spikes were used to achieve initial concentrations of $1 \cdot 10^{-9}$ mol·L^{-1} and $3 \cdot 10^{-11}$ mol·L^{-1} of the elements, respectively. GO was separated by centrifugation at 20000xg for 15 min while MGO by a magnet. Pu and Am in the solution were determined after radiochemical separation using the UTEVA and TRU resins (Eichrom Industries), ^{242}Pu and ^{243}Am were used as tracers in the separation procedures. Elements were measured using ICP-MS.

In experiments with Cs to investigate the effect of coexisting ions, the 100 mg L^{-1} of CsCl in seawater 35 ‰, 100 mg L^{-1} of CsCl in 100 mg L^{-1} of KCl and 100 mg L^{-1} of CsCl solutions were used. GO was separated by centrifugation at 20000xg for 15 min while magnetic GO composites – with a magnet. Cs solutions were traced with ^{134}Cs and Cs activity concentrations were measured by gamma spectrometry using a HPGe detector (resolution 1.9 keV/1.33 MeV and efficiency 42 %).

The ACS reagent grade or higher-grade chemicals and deionized (Elix, Milipore) or Milli-Q (Millipore Milli-Q Synthesis A-10) water were used to prepare all solutions and in all experiments.

2.4. Uncertainty, sorption efficiency and sorption capacity calculations

The sorption capacity of sorbent was calculated using this formula:

$$q_e = \frac{(C_0 - C_e) \cdot V}{m} \quad (2.1),$$

q_e – the equilibrium sorption capacity of the sorbent (mg g^{-1}) (or mol g^{-1});
C_0 - the initial concentration of target ions (mg L^{-1}) (or mol g^{-1});
C_e - the concentration at equilibrium of target ions (mg L^{-1}) (or mol g^{-1});
V - the volume of target ions solution (L);
m - the weight of the used sorbent (g).

The sorption efficiency - uptake was calculated:

$$Uptake\ (\%) = \frac{C_0 - C_e}{C_0} \times\ 100\ \% \qquad (2.2),$$

Uptake – sorption efficiency (%).

The standard uncertainty was calculated according to the formula:

$$u^2(X) = u_1^2 + \cdots + u_n^2 \qquad (2.3),$$

$$u(X) = \sqrt{\sum_{i=1}^{n} u_i^2} \qquad (2.4),$$

u_i – sources of uncertainty: measurements, sample preparation, devices uncertainty, and other.

3. RESULTS AND DISCUSSION

3.1. Study of heavy metal and radionuclide sorption to graphene oxide

The sorption experiments were carried with radionuclides and heavy metals in normal conditions. All used reagents were analytical grade. The solutions were prepared using ultra-pure water. Synthesized sorbents were cleaned of possible contaminants and dried for accurate dosing. Initially, sorption experiments were carried out with heavy metals, since in fact there are their radioactive isotopes. For the research, metals such as nickel (Ni^{2+}), cobalt (Co^{2+}), lead (Pb^{2+}) and copper (Cu^{2+}) were taken. The basis for this choice was many experiments, exemplified in the literature. Figure 3.1. shows the effect of initial concentrations on heavy metals (Co^{2+}, Cu^{2+}, Ni^{2+} and Pb^{2+}) sorption to synthesized graphene oxide.

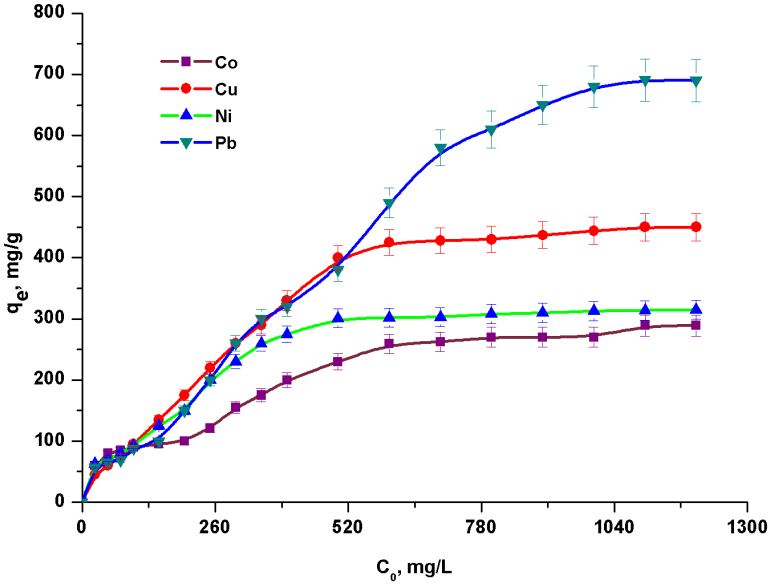

Fig. 3.1. The effect of initial concentrations on heavy metals (Co^{2+}, Cu^{2+}, Ni^{2+} and Pb^{2+}) sorption to synthesized graphene oxide

The maximum sorption capacities of heavy metals to GO were reached as it is presented in the figure 3.1. We can see that they are different for each of a metal, for example for Co^{2+} it is just a 289 $mg \cdot g^{-1}$, for Ni^{2+} - 315 $mg \cdot g^{-1}$, for Cu^{2+} - 450 $mg \cdot g^{-1}$ and finally for Pb^{2+} it is 691 $mg \cdot g^{-1}$. The graphene oxide concentration was 1 $mg \cdot ml^{-1}$.

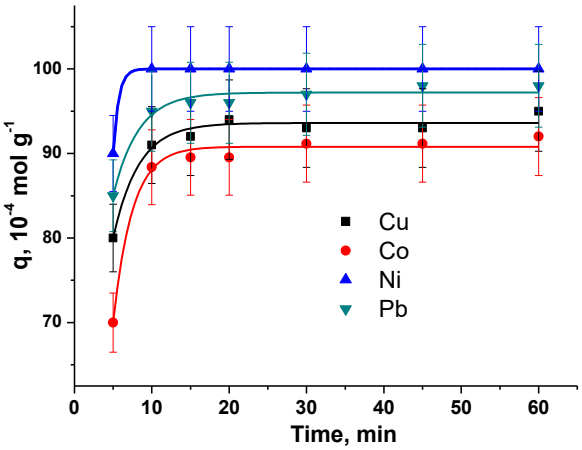

Fig. 3.2. Sorption kinetics of Cu^{2+}, Co^{2+}, Ni^{2+} and Pb^{2+} to graphene oxide

Kinetic data were fitted to the pseudo-first-order kinetic model:

$$q_t = q_e(1 - e^{-k_{ad}t}) \quad (3.1)$$

where q_t and q_e are the studied element concentrations (μmol·g^{-1}) at time t and equilibrium, respectively, while k_{ad} (min^{-1}) is the pseudo-first-order rate constant. The kinetic parameters showed that obtained data well fited the pseudo-first-order equation (table 3.1):

Table 3.1. The kinetic constants and their correlation coefficients for heavy metals sorption

	Cu^{2+}	**Co^{2+}**	**Ni^{2+}**	**Pb^{2+}**
R^2	0.998	0.998	0.999	0.999
q_e	94.3±0.4	91.7±0.5	100.0±0.3	97.6±0.5
k_{ad}	0.37±0.01	0,29±0.01	0.46±0.01	0.41±0.01

Studying the toxic element removal from a solution, one of the important characteristics is the reaction kinetics. Figure 3.2. presents the effect of heavy metal ion sorption to GO on contact time. All elements showed a fast sorption to a sorbent. The quantity of sorbed Cu^{2+}, Co^{2+}, Ni^{2+} and Pb^{2+} after 5 minutes varied from 70 to 90 %. The equilibrium with the sorption level from 90 % to 100 % was reached after 10 – 60 minutes of contact time with a sorbent. The pH has decreased from 5.4±0.1 (initial pH value) to 3.3±0.1 (at the end of sorption experiments).

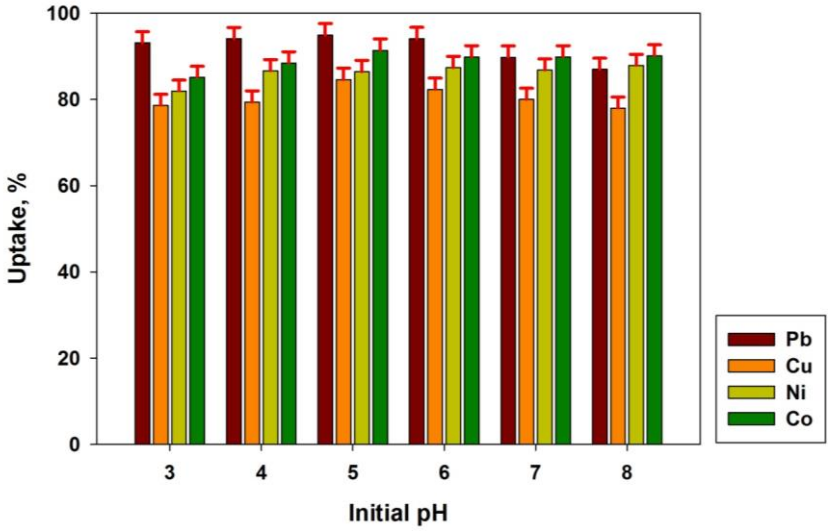

Fig. 3.3. Sorption of Cu^{2+}, Co^{2+}, Ni^{2+}, Pb^{2+} to graphene oxide depending on initial pH

The graph in figure 3.3. shows the effect of initial pH of the GO sorption of heavy metals. The concentration C (Cu^{2+}, Co^{2+}, Ni^{2+}, Pb^{2+}) of metal cations was 100 mol·L^{-1}. Contact time - 24 hours. We can see that in all range of studied initial pH the uptake is over 80 % for all tested elements. The especially small variations in the range from 90 % to 95 % were observed for Ni uptake. On the other hand, for Cu the value of 90- 92 % is reached when initial pH was from 5 to 6. Values of uptake for Pb^{2+} was the best when initial pH was also from 5 to 6. The largest amount of Co^{2+} up to 93 % was sorbed when initial pH was ~ 8.

Effects of initial pH on sorption for radionuclides to the GO based nanosorbents are presented in Fig. 3.4. As it can be seen, the maximum sorption was achieved at the initial pH 5 and was 88 %. Throughout the range of values studied, the sorption occurs with positive dynamics. This indicates the ability of the sorbent to react with metals under severe conditions. Throughout the entire study range the sorption values above 75 percent for (Pu) plutonium and over 85 percent for Am. We have measured the pH after sorption experiments to investigate the changes in the samples, as a result we`ve got the decrease of pH values.

The Am (III) and Pu (IV) uptake by GO and MGO1 and MGO2 depending on pH showed wide variations (Fig. 3.4.). The maximum uptake of Pu and Am by GO was found at the initial pH values of 3-5 (Fig 3.4. A) and at the initial pH value of 7 for MGO1, whereas an increase of Pu and Am

adsorption from 60 % to ≈ 100 % was observed for MGO2 in the pH range from 3 to 9 (Fig.3.4. B, C). It can be seen that the final pH values varied to a different extent from initial ones. A significant decrease in final pH values which were close to the GO pH_{pzc} value of 3.0 – 3.4 indicated the ion exchange mechanism, sorption of elements to –COOH and –OH groups and release of protons into solution in all experiments with GO (Fig. 3.4. A). However, the pH of liquid-phase was quite stable and the uptake increased at the pH value higher than the MGO GO pH_{pzc} value of 4.5 showing the involvement of different sorption groups into sorption process (Fig. 3.4. B, C).

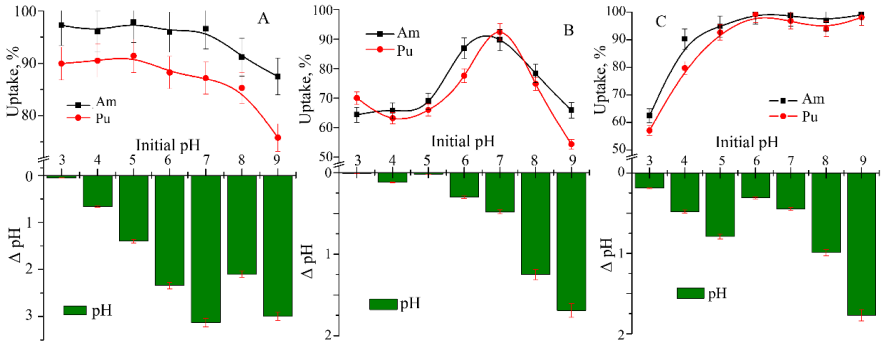

Fig. 3.4. Effect of pH on Am and Pu (IV) sorption to graphene oxide (A), MGO1 (B) and MGO2 (C), background electrolyte 0.01 mol·L^{-1} $NaClO_4$, contact time 1440 min.

The main difference in sorption behavior of Pu and Am can be attributed to the availability of different sorption sites on the sheets of the GO, MGO1 and MGO2. MGO1 contained lower concentration of iron and accordingly a lower amount of magnetite nano-particles on the GO surface. The surface of its sheets was partly covered with nano-magnetite particles and both sorption sites characteristic of GO and magnetite were available for the uptake of radionuclides.

The observed variations in the uptake of Pu and Am are most probably related to a charge redistribution of the GO surface. MGO2 sorbent contained higher concentration of Fe and it was uniformly covered with magnetite nano-particles. The sorption sites typical of magnetite were predominant, and for this reason a different pattern of Pu and Am sorption was observed. The sorption mechanism in this case should be similar to sorption of Pu and Am on magnetite.

3.2. Cs sorption to graphene oxide and Prussian blue nanocomposites

Adsorption isotherms provide important information about sorption mechanisms of studied elements. Distribution of metal ions between the liquid-phase and solid-phase can be described by Langmuir and Freundlich models. The Langmuir isotherm applicable to monolayer adsorption onto the surface contains a finite number of identical adsorption sites. The model assumes uniform energy distribution and no transmigration of sorbate in the plane of the surface (Langmuir, 1916).

The Langmuir model in the linear form can be represented as follows:

$$\frac{C_e}{q_e} = \frac{1}{b \cdot Q_{max}} + \frac{C_e}{Q_{max}} \qquad (3.2)$$

where C_e - the equilibrium concentration of metal ions (mg·L^{-1})(or mmol L^{-1}), q_e - the amount of metal ions sorbed by sorbent (mg·g^{-1}) (or mmol L^{-1}), b - the Langmuir constant related to the energy of adsorption (L·mg^{-1}) (or L mmol^{-1}) and Q_{max} is the maximum adsorption capacity (mg·g^{-1}) (or mmol g^{-1}).

The linearized Freundlich model is:

$$ln\, q_e = ln\, k + \frac{1}{n} ln\, C_e \qquad (3.3)$$

where *1/n* is the Freundlich intensity parameter and *k* indicates the adsorption capacity of sorbent.

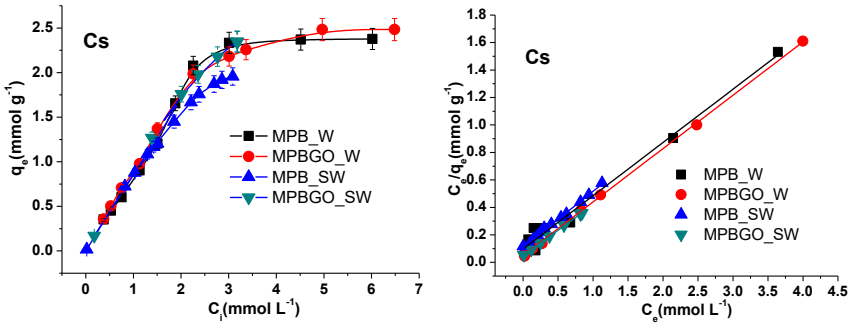

Fig. 3.5. Initial concentration of Cs^+ versus q_e and Langmuir isotherms for adsorption of Cs^+

Adsorption of Cs ions at different initial concentrations of CsCl was studied for 24 h at room temperature and pH = 7. In addition, Cs adsorption was studied at different initial CsCl concentrations in seawater solution of 35‰ at pH = 7. The cesium adsorption isotherms are presented in Fig.3.5. and the isotherm constants and correlation coefficients – in Table 3.2.

Table 3.2. Langmuir isotherm constants and their correlation coefficients for Cs sorption to MPB and MPBGO

Composite	R^2	b	Q_{max}, mg g^{-1}	Q_{max}, mmol g^{-1}
MPB_W	0.981	0.030	347±16	2.58±0.12
MPBGO_W	0.999	0.057	343±14	2.57±0.09
MPB_SW	0.996	0.027	333±18	2.46±0.09
MPBGO_SW	0.999	0.076	362±14	2.72±0.08

Cs^+ cation isotherms well fitted to the Langmuir model (R^2 ranged from 0.981 to 0.999). Q_{max} values varied from 333 mg·g^{-1} to 362 mg·g^{-1} and were significantly higher than those found in other studies. The Q_{max} values obtained for Cs adsorption to MPB and MPBGO from pure water ranged within the uncertainties. The highest Q_{max} values were found for the MPBGO composites in experiments with seawater. It can be attributed to the improved selectivity of MPBGO towards Cs ions.

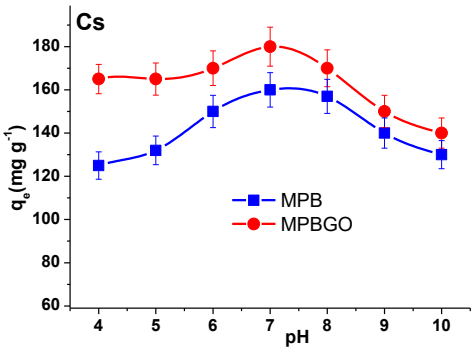

Fig. 3.6. Effect of pH on Cs sorption to MPB and MPBGO nanocomposites.

Variation of pH values can significantly affect the sorption capacities of sorbents. The effect of pH was studied at different pH values from 4 to 10 in 200 mg L^{-1} CsCl solutions (Fig. 3.6.). The decrease in q_e values was observed under the strongly acidic and alkaline conditions, which is consistent

with the observations of other researchers (Yang et al., 2014). This phenomenon can be explained by PB dissolution under acidic conditions and decomposition under alkaline ones. The highest q_e values were found under neutral conditions at pH =7.

To estimate possible effects of coexisting ions on Cs sorption to composites the sorption experiments were conducted using seawater 35 ‰ and 200 mg L^{-1} KCl solutions at pH = 7 for 24h. The obtained q_e values are presented in Fig. 3.6. The results indicated a decrease in Cs ion adsorption on the MPB composite, while rather small variations, which were within the limits of the uncertainties, for sorption of Cs to MPBGO were found. Thus, the MPBGO nanocomposite can effectively sorb Cs even at high concentrations of K^+, Na^+ and other ions naturally occurring in seawater. It is very well known that due to similar hydration radii, potassium ions can compete with Cs for sorption sites on the PB surface. The effect of coexisting ions was usually related to the hydration radii of cations and it decreased in the order as follows: Cs^+ (3.25 Å), K^+ (3.3 Å), Na^+ (3.6 Å), Ca^{2+} (4.1 Å), Mg^{2+} (4.25 Å) (Conway, 1981).

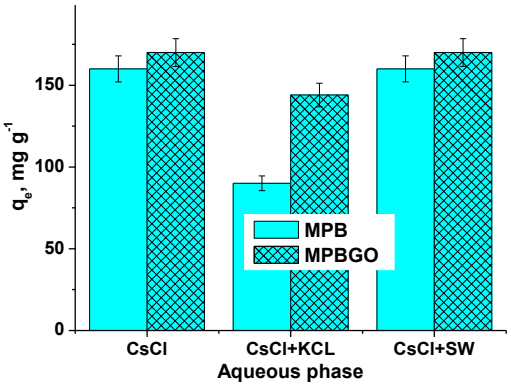

Fig. 3.7. Effect of coexisting ions on Cs adsorption.

It is believed that the adsorption mechanism of Cs is associated with the ion exchange between potassium and cesium, which occurs without changes in the crystalline lattice of Prussian blue (Loos-Neskovic et al., 2004; Ca & Cox, 2004). Another possible mechanism of adsorption is linked to physical sorption, which is associated with a cationic trapping and depends on variations in the lattice of the crystal structure (Avramenko et al., 2011). The improved adsorption selectivity observed during this study supports the physical sorption mechanism. Characterization of synthesized nanocomposites indicated that they were covered with PB. Thus, sorption properties of composites should be similar to those of PB, and the sorption

groups present on the PB surface are responsible for the enhanced selectivity of the MPB and MPBGO.

Experiments carried out with natural seawater indicated a high efficiency of MPBGO for adsorption of Cs ions. ^{137}Cs was extracted from 30 L seawater samples collected in the Baltic Sea. ^{134}Cs was applied as the yield tracer in the pre-concentration procedure. The activity concentrations measured using gamma spectrometry ranged from 20 to 30 Bq m^{-3}. The adsorption efficiency of MPBGO for Cs in natural seawater was found to be about 100 %. Higher adsorption capacities obtained as compared with the published data can be explained by the structure of nanocomposites synthesized during this study.

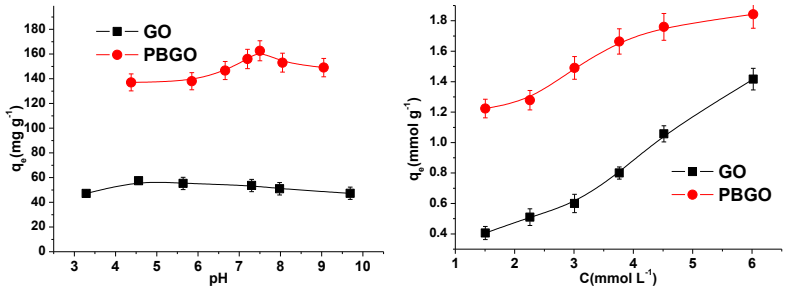

Fig 3.8. Effect of initial pH and concentrations on Cs sorption to graphene oxide and comparison with Prussian blue graphene oxide nanocomposite

Experiments on Cs (I) sorption using graphene oxide and Prussian blue graphene oxide composite have been carried. The results are presented in figure 3.8. As we can see, the left graph shows the effect of initial pH on Cs sorption by the synthesized nanocomposites. The GO showed stable results throughout the tasted pH range with sorption from 45 to 58 mg·g^{-1}. This suggests that graphene oxide can effectively sorb radionuclide under various conditions like in acidic or alkaline solutions. Graphene oxide based nanocomposite, the PBGO, showed a better sorption effectiveness under the same conditions. It can be seen from the graph that this compound sorbed 155 mg·g^{-1} of Cs (I) at initial pH = 7.5. This shows that the PBGO composite in neutral medium is 2.67 times more efficient than the graphene oxide. The adsorption rate decreases under alkaline and acid conditions and, accordingly, sorbs 145 and 140 mg·g^{-1}.

The graph on the right shows the effect of initial concentrations on Cs adsorption to GO and PBGO nanocomposite. The Prussian blue graphene oxide composite sorbed 3 times more Cs (I) than GO at the same sorbent concentration of 1.5 mmol·L^{-1}. The increasing concentration improves the rate

of adsorption. The increase of Cs concentration by 4 times to 6 mmol·L^{-1} led to increase of its adsorption to GO by 3.25 times to 1.4 mmol·g^{-1}. The increase of Cs concentration by a factor of 1.5 led to its enhanced adsorption on PBGO up to 1.8 mmol g^{-1}.

3.3. Sorption of metals and radionuclides to graphene oxide and chitosan graphene oxide nanocomposite comparison

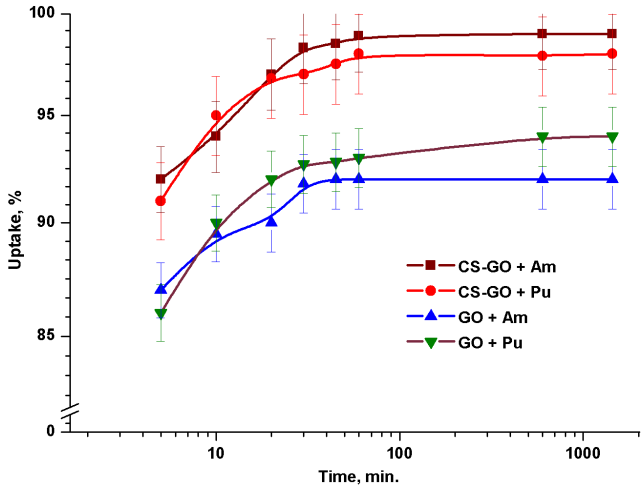

Fig. 3.9. Effect of contact time on Am and Pu adsorption on graphene oxide and chitosan graphene oxide nanocomposites

A fast adsorption of radionuclide to sorbents has been observed as it showed in Fig 3.9. The equilibrium was reached after 10 - 60 minutes. As we can see both of sorbents show the good performance while contact time is not long, for example if we'll got some sample to remove radionuclide, it would be enough a 10 minutes contact for its clean out.

Data on the sorption kinetics presented in figure 3.9. have indicated the fast adsorption of Am and Pu both to the GO and CSGO. The amount of Am and Pu sorbed to GO after 5 min. was 87 % and 86 %, while that to CSGO was 93 % and 92 %, respectively. The similar amounts of Am and Pu of 97 % and 98 % as well as 99 % and 97 % were found to be sorbed to GO and CSGO, respectively, after 90 min. contact time. Thus, both GO and CSGO sorbents are appropriate for Pu and Am removal from contaminated solutions, nevertheless, faster kinetics is characteristic of the CSGO composite.

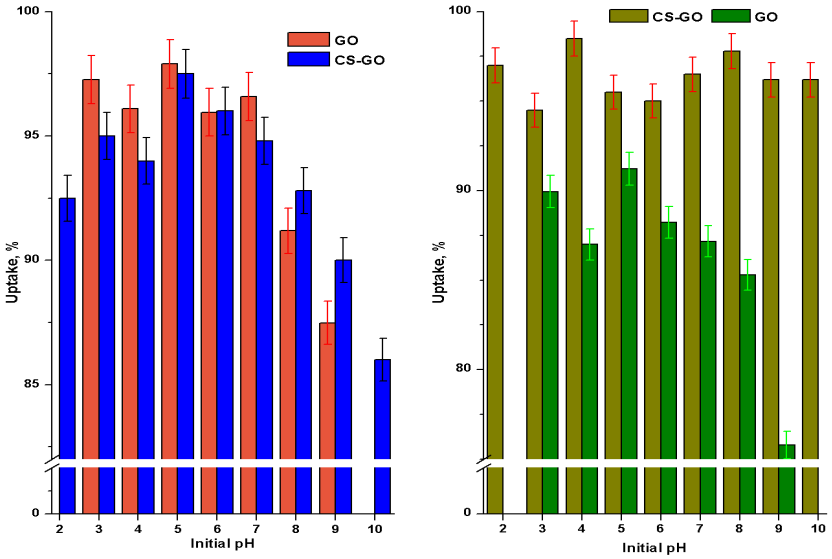

Fig. 3.10. Effect of pH on Am (left) and Pu (right) sorption to graphene oxide and comparison to chitosan graphene oxide composite

The chitosan graphene oxide composite was used to reach the better sorption for radionuclides. The experiment was also made to investigate the pH dependence of Am and Pu (IV) sorption (Figure 3.10.). It has been found that CSGO composite has a better adsorption ability for Pu isotopes as compared to GO. Sorption of radionuclides to GO and CSGO was studied in a wide range (from 2 to 10) of the initial pH values (Figure 3.10). The maximum values of 99 % and 98 % for Pu and Am sorption to CSGO were observed at pH of 4 and 5, respectively. In addition, a decrease in adsorption of Pu and Am on GO from maximum values of 98% to 87% and from 92 % to 80 % was found. The sorption experiments indicated the better adsorption ability of CSGO for Am and Pu radionuclides. The experiments showed the better adsorption ability for Am isotopes, where uptake was more than 90 % in all tested pH range. For Pu isotopes it was also not bad, as we can see the uptake was more than 80 % from initial pH 3 to 8, for higher pH it decreases.

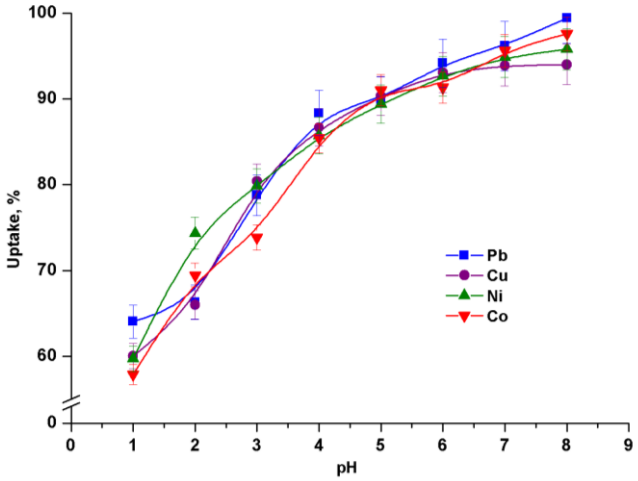

Fig. 3.11. Effect of pH on Pb^{2+}, Cu^{2+}, Ni^{2+} and Co^{2+} sorption to chitosan graphene oxide composite

Also, CSGO nanocomposite was used to investigate the sorption for heavy metals. The experiment was made to investigate the pH dependence of Pb^{2+}, Cu^{2+}, Ni^{2+} and Co^{2+} sorption (Figure 3.11.). It has been found that CSGO composite sorbs heavy metals in all range of tested initial pH as it showed. Maximum sorption ability for each metal was from 7 to 8 pH. The higher pH values were not studied because of the metal ability to make metals precipitate creating salts. As it is seen in the figure 3.11., sorption was performed from initial pH 1 and reached the value of 60 % of uptake. At all range of initial pH from 1 to 6 the sorption for metals increased properly to 90 % of uptake.

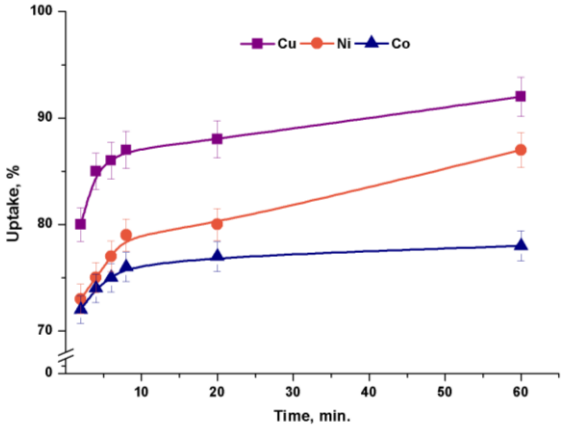

Fig.3.12. Effect of contact time on Cu^{2+}, Co^{2+}, Ni^{2+} sorption to chitosan graphene oxide nanocomposite

A fast adsorption of heavy metals to CSGO sorbent has been observed as it showed in figure 3.12. The equilibrium was reached after 10 minutes for Co^{2+}. For Ni^{2+} and Cu^{2+} the equilibrium was reached after 30 minutes of contact time. As we can see, both of sorbents, the GO studied before and CSGO showed the good performance while contact time is not long, for example if we'll got some sample to remove radionuclide or heavy metals, it would be enough a 30 - 60 minutes contact for its clean out.

3.4. Effect of pH on sorption of metal ions and radionuclides using the graphene oxide and GO based composites

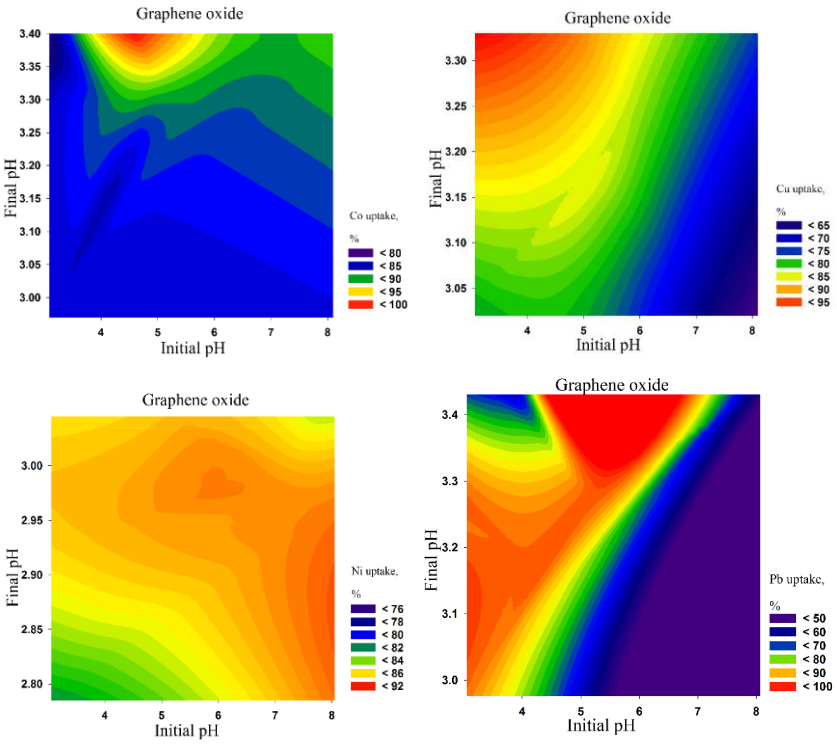

Fig. 3.13. pH effect on Cu^{2+}, Co^{2+}, Ni^{2+} and Pb^{2+} sorption to graphene oxide

A rather high uptake for Am can be expected at all initial pH values, meanwhile the acidic pH region from 3 to 6 was more favorable for sorption of Pu (IV) isotopes. Two uptake plots observed for the MGO1 (with a low amount of magnetite) can be interpreted as adsorption to a different type of sites present on GO sheets suitable for sorption in the acidic region and

available on magnetite particles for the uptake at the higher pH (Fig. 3.13). Nonetheless, one sorption plot was found to be characteristic of MGO2 sorbent with a high content of magnetite since sorption sites on the GO sheets were suppressed by magnetite particles.

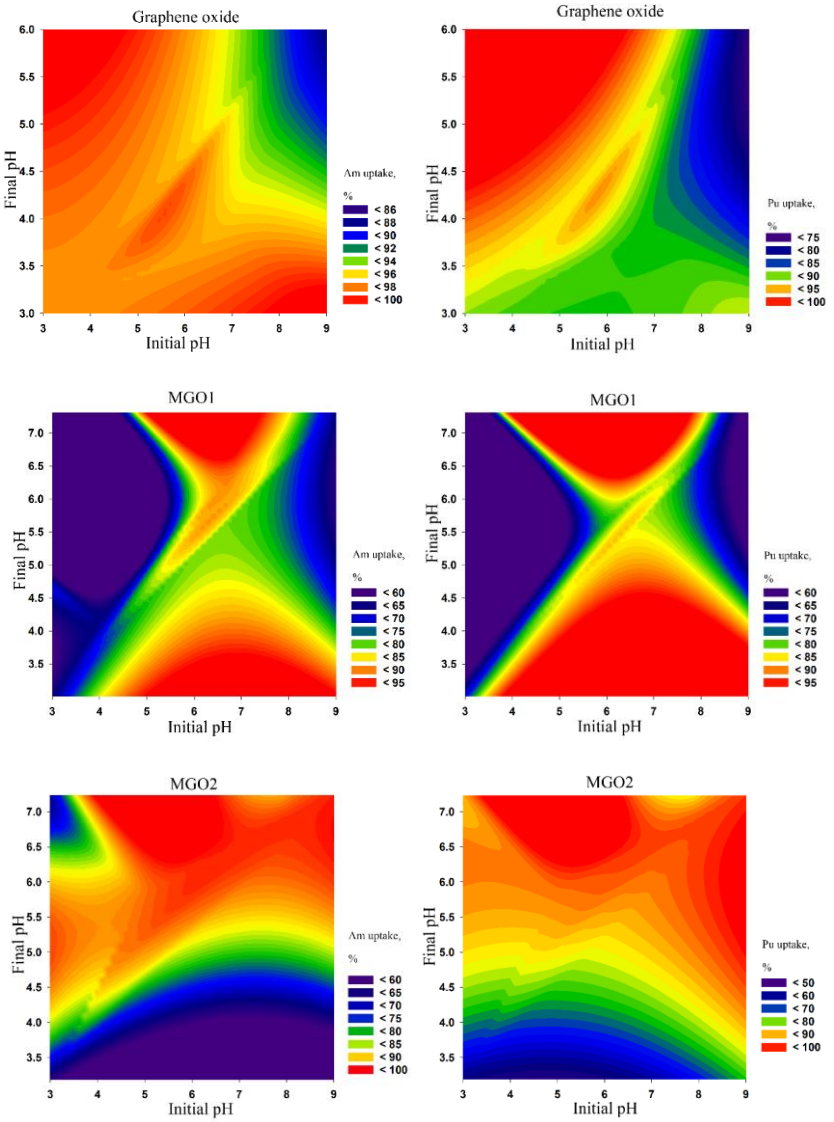

Fig. 3.14. pH effect on Am and Pu sorption to GO, MGO1, MGO2

The analysis of data from Fig 3.14. three sets of experiments were performed to calculate variation in the uptake of studied elements by three sorbents (Fig. 3.14). Results indicated a rather high adsorption potential under acidic

conditions for Cu^{2+}, Pb^{2+} and Co^{2+} while Ni^{2+} showed a high uptake at all initial pH values.

3.5. Natural clay for radionuclide removal

Three well-characterized samples from the industrial exploitation site Šaltiškiai in North Lithuania were used to study Pu(V) sorption kinetics and oxidation state distribution in natural clay systems. The laboratory batch method (slightly modified by measurement of pH before and after the sorption experiment, as well as by analysis of Pu oxidation state (EPA, 1999)) was used in this study.

The bonding (speciation) of sorbed Pu in the solid-phase was studied using SE procedures with the following fractions and extractants: F1 – 0.1 mol·L^{-1} $MgCl_2$ (exchangeable); F2 – 1 mol·L^{-1} CH_3COONH_4, 25 % CH_3COOH (carbonate bound) , F3 – 0.04 mol·L^{-1} $NH_2OH{\cdot}HCl$, 25 % CH_3COOH (oxides), F4 – 30 % H_2O_2, pH 2 (HNO_3) (organic matter), F5 – 4 mol·L^{-1} HNO_3 (acid soluble) F5 – 1:3 HNO_3 : HCl (residual). The composition of clay mineral coatings and their leaching during the sequential extraction procedures were investigated by means of the Mössbauer spectroscopy and X-ray diffraction.

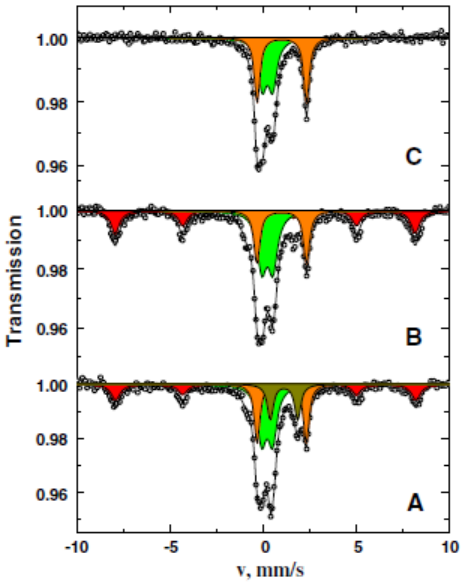

Fig. 3.15. Mössbauer spectra of clay minerals used in sorption experiments

The Mössbauer spectra of the samples were recorded using the Mössbauer spectrometer operating in transmission geometry in a constant

acceleration mode. The source of ^{57}Co in Rh matrix was used. Mössbauer data (Fig. 3.15.) revealed a different composition of clays reflected by iron atom distribution as follows: A) S clay (Mössbauer spectra area is attributed to Fe^{2+} – 18 %, Fe^{3+} – 43 %, $FeCO_3$ – 13 %, α-Fe_2O_3 – 26 %); B) 6 clay (Fe^{2+} – 19 %, Fe^{3+} – 47 %, α-Fe_2O_3– 34 %); C) 7 clay (Fe^{2+} – 37 %, Fe^{3+} – 63 %). The measurements carried out after every step of the SE showed leaching of siderite mineral from clay coatings (Fig. 3.16).

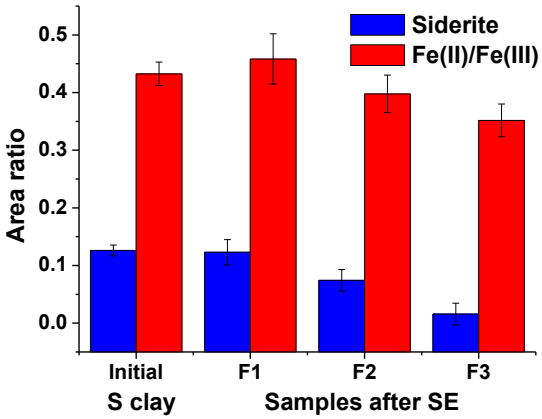

Fig. 3.16. Variations of Siderite and Fe (II)/Fe (III) in S clay samples during the sequential extraction (SE) procedure

Siderite ($FeCO_3$) was washed out from the surface of clay particles with the carbonate fraction (F2), and the other with oxides (F3). This can be attributed to the layered structure of mineral coatings. It appears that the siderite surface was partly covered with iron oxides and they protected it from dissolution during the extraction of carbonates. Similar results were obtained in our previous studies using a different protocol of the SE procedure.

The X-ray diffraction (XRD) analyses were conducted by means of a D8 (Bruker AXS) X-ray diffractometer. Clay particles of < 1 μm in size for analyses were separated by settling techniques. Three spectra of each sample of interest were recorded using: 1) deposited on glass and dried clay minerals; 2) calcinated at 600°C in air atmosphere; 3) treated with ethylene glycol for 12 h. Chemical analyses and the interactive Diffract. Suite EVA version 1.4 software package (2010), using the powder diffraction file database associated with the program, were applied to the phase identification. XRD data showed the presence of Illite ($K_{0.65}Al_{2.0}[Al_{0.65}Si_{3.35}O_{10}](OH)_2$), Kaolinite ($Al_2(Si_2O_5)(OH)_4$), Montmorillonite ($(Na,Ca)_{0.33}(Al,Mg)_2(Si_4O_{10})(OH)_2$·

nH_2O), Clinochlore $((Mg,Fe^{2+})_5Al(AlSi_3O_{10})\cdot(OH)_8$). No significant effect of sequential extraction treatment on the minerals was observed.

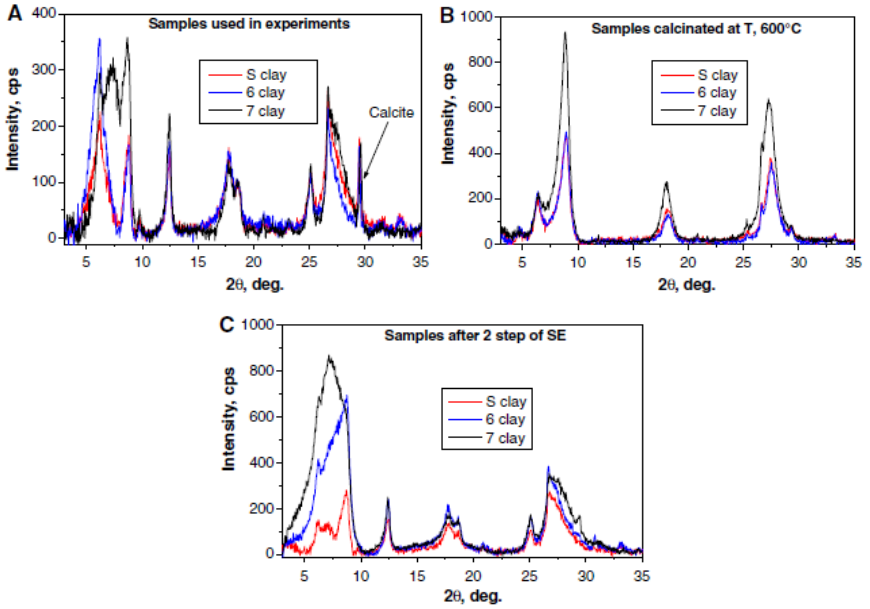

Fig. 3.17. XRD spectra of clay minerals used in sorption experiments

The complete removal of calcite mineral after the second step of SE was determined in samples of clay S and clay 6 while a small amount was found to be not washed out from sample clay 7 (Fig. 3.17). The total amount of calcite (7 – 34.0 % > S – 19.8 % > 6 – 19.0 %) and TOC (7 – 0.062 % > 6 – 0.035 % > S – 0.034 %) varied in the studied samples.

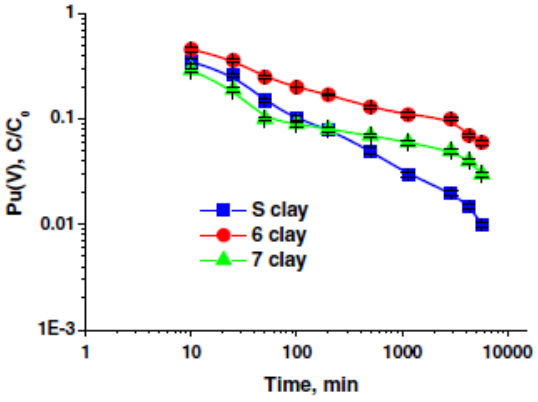

Fig. 3.18. Pu (V) sorption kinetics to three natural clays from groundwater as a function of contact time

Solutions and SE eluates were evaporated and wet-ashed using HCl, $HClO_4$, HNO_3, H_2O_2. Pu isotopes after radiochemical separation using the UTEVA and TRU (Eichrom Industries) were measured by alpha spectrometry or ICP-MS. ^{242}Pu was used as a tracer in the separation procedure.

The kinetics of Pu (V) sorption from natural groundwater to clays S, 6 and 7 with different carbonate and iron minerals in coatings was studied using Mössbauer spectroscopy (Fig. 3.15). A slightly better Pu (V) uptake by clay S was observed (Fig. 3.18.). Experimental data obtained from the kinetic sorption experiments were used in modelling. The data were evaluated by fitting with six different types of kinetic models, derived for the following six control processes: mass transfer (DM), film diffusion (FD), diffusion in the inert layer (ID), diffusion in the reacted layer (RLD), chemical reaction (CR) and gel diffusion (GD).

Table 3.3. Sorption kinetic equations

Control process	**Model**	Differential equation
Mass transfer	*DM*	$dq/dt = K_{DM} \cdot (q^* - q)$
Film diffusion	*FD*	$dq/dt = K_{FD} \cdot (C - C^*)$ $K_{FD} = 3 \cdot D/(\delta \cdot R \cdot h_s)$
Diffusion in inter layer	*ID*	$dq/dt = K_{ID} \cdot (C - C^*)/\{[1 - (q/q^*)]^{-1/3} - 1\}$ $K_{ID} = 3 \cdot D/(R^2 \cdot h_s)$
Diffusion in reacted layer	*RLD*	$dq/dt = K_{RLD} \cdot (q^* - q)/\{[1 - (q/q^*)]^{-1/3} - 1\}$ $K_{RLD} = 3 \cdot D/(R^2 \cdot h_s)$
Chemical reaction (taking place on reaction zone) e.g., 1st order reversibel reaction	*CR*	$dq/dt = K_{CR} \cdot r_{CR} \cdot [1 - (q/q^*)]^{2/3}$ $K_{CR} = 3/(R \cdot h_s)$ $r_{CR} = k_{CR} \cdot (C - C^*)$
Gel diffusion	*GD*	$dq/dt = K_{GD} \cdot [(q^* - q_0)^2 - (q - q_0)^2]/(q - q_0)$ $K_{GD} = D \cdot \pi^2/(2 \cdot R^2)$

C - concentration of the component in the solution at time *t*, *C**- equilibrium concentration of the component in the solution corresponding to the concentration of the component in solid phase at time *t*, *q* - concentration of the component in the soil at time *t*, q^* - equilibrium concentration of the component in the soil corresponding to the concentration of the component in liquid phase at time *t*, q_0 - starting concentration of the component in the soil, *t* - time, *D* - diffusion coefficient of the component, K_{DM} - mass transfer coefficient, K_{FD}, K_{ID}, K_{RLD}, K_{CR}, K_{GD} - overall kinetic coefficients, k_{CR}- kinetic coefficient of the chemical reaction, r_{CR} - rate of the chemical reaction, *R* - mean radius of the soil particle, h_s - specific mass of the soil, δ - thickness of the liquid film on the surface of the soil particle.

The differential model equations describing these control processes are summarized in Table 3.3. The fitting of experimental data proceeded by means of non-linear regression procedure in an iteration cycle from which it was possible to determine the K_{DM}, K_{FD}, K_{ID}, K_{RLD}, K_{CR} and K_{GD} values. As a fitting criterion, reflecting the agreement between the calculated and experimental values, the *WSOS/DF* (Weighted Sum of Squares divided by the Degrees of Freedom) quantity was calculated. Generally, the agreement is acceptable if $0.1 \leq WSOS/DF \leq 20$.

Table 3.4. Fitting of experimental data by six kinetic model – values of WSOS/DF

Solid phase (pH of solution)	**Kinetic model**					
	DM	*FD*	*ID*	*RLD*	*CR*	*GD*
S Clay (pH 7,5 – 8)	52,70	54,30	5,22	10,30	53,40	12,30
6 Clay (pH 7,5 – 8)	23,70	28,10	4,62	4,68	22,20	9,76
7 Clay (pH 7,5 – 8)	59,70	72,60	9,36	8,20	68,10	9,88

The values of *WSOS/DF* obtained during the fitting procedures for all experiments are presented in Table 3.4. The data suggest that diffusion in the inert layer is the control process in the sorption experiments with clay S since the best fits, i.e. the lowest values of *WSOS/DF*, were obtained with the ID kinetic model, while for clay 6 and clay 7 both control processes, diffusion in the inert layer and diffusion in the reacted layer, were found to be suitable.

Characteristic parameters of the sorption kinetics obtained from the model curves are presented in Table 3.5. Kinetic coefficients increased in the following sequence: clay 6 (RLD) > clay 7 (RLD) >clay S (ID)>clay 6 (ID) > clay 7 (ID). The highest Pu K_d ($1.10 \cdot 10^5$ mL·g^{-1}) values for clay S were expected due to the presence in the samples of strong reductant siderite. Pu K_d values for clays 6 and 7 were found to be $3.9 \cdot 10^4$ mL·g^{-1}. Pu K_d values obtained in experiments with Pu (IV) and clay minerals ranged from $8.39 \cdot 10^3$ mL·g^{-1} to $2.35 \cdot 10^4$ mL·g^{-1}. The kinetic coefficients in experiments with Pu (IV) varied from $3.30 \cdot 10^{-2}$ min^{-1} to 2.31 min^{-1}, while for Pu (V) they ranged from $1.78 \cdot 10^{-1}$ min^{-1} to 1.06 min^{-1}.

Table 3.5. Results of modeling of sorption kinetics of Pu on clays S, 6 and 7 from natural groundwater

Exp. No.	Starting Concentration of Pu, [mol/l]	Control process	Kinetic coefficient [min^{-1}]	Half-time of sorption (approx.) [min]*	K_d [mL/g]	*WSOS/ DF*
Clay S	$1{,}00 \cdot 10^{-10}$	*ID*	$1{,}78 \cdot 10^{-1} \pm 3{,}72 \cdot 10^{-4}$	< 5	$1{,}10 \cdot 10^{5} \pm 5{,}6 \cdot 10^{3}$	5,22
Clay 6	$1{,}00 \cdot 10^{-10}$	*ID*	$6{,}90 \cdot 10^{-1} \pm 6{,}29 \cdot 10^{-2}$	< 1	$3{,}59 \cdot 10^{4} \pm 1{,}8 \cdot 10^{3}$	4,62
Clay 6	$1{,}00 \cdot 10^{-10}$	*RLD*	$3{,}92 \cdot 10^{-5} \pm 6{,}38 \cdot 10^{-7}$	< 1	$3{,}59 \cdot 10^{4} \pm 1{,}8 \cdot 10^{3}$	4,68
Clay 7	$1{,}00 \cdot 10^{-10}$	*ID*	$1{,}06 \pm 4{,}42 \cdot 10^{-3}$	< 1	$3{,}35 \cdot 10^{4} \pm 1{,}7 \cdot 10^{3}$	9,36
Clay 7	$1{,}00 \cdot 10^{-10}$	*RLD*	$4{,}49 \cdot 10^{-5} \pm 3{,}39 \cdot 10^{-7}$	< 1	$3{,}35 \cdot 10^{4} \pm 1{,}7 \cdot 10^{3}$	8,20

* Uncertainties corresponding to the determination of kinetic coefficient represent one standard deviation (k=1).

The oxidation state distribution data obtained for all three systems are presented in Fig. 3.19. The fast reduction of Pu (V) introduced in the systems was observed. A small amount of Pu (V) in the liquid-phase was found for all three clay types (Fig. 3.19, A, C, E), whereas in the solid-phase it was detected only in experiments with clay S and clay 6 (Fig. 3.19. B, D). Pu (VI) was not found in any of the samples. A rather similar Pu oxidation state distribution was observed in the solid-phase of clays S and 6 and a slightly higher amount of Pu (IV-pol) was found in those of clay 7. The amount of Pu (III, IV) decreased in the sequence of 6 > S > 7 in the solid-phase. In the liquid-phase Pu (III) was not detected while the amount of Pu (IV) decreased in a similar sequence. The fast kinetics and highest K_d values estimated for Pu (V) sorption to S clay can be attributed to the fast reduction by siderite and can be an indication that Pu (V) reduction to Pu (IV) was the main process controlling Pu sorption to clay minerals. Higher percentage of Pu (IV) found in the solid- and in the liquid-phases in the experiment with clay 6 most probably can be explained by high affinity of Pu (IV) and Pu (IV-pol) to iron oxide surfaces, and/or complexation Pu (IV) due to changes in the composition of the liquid-phase during the experiment.

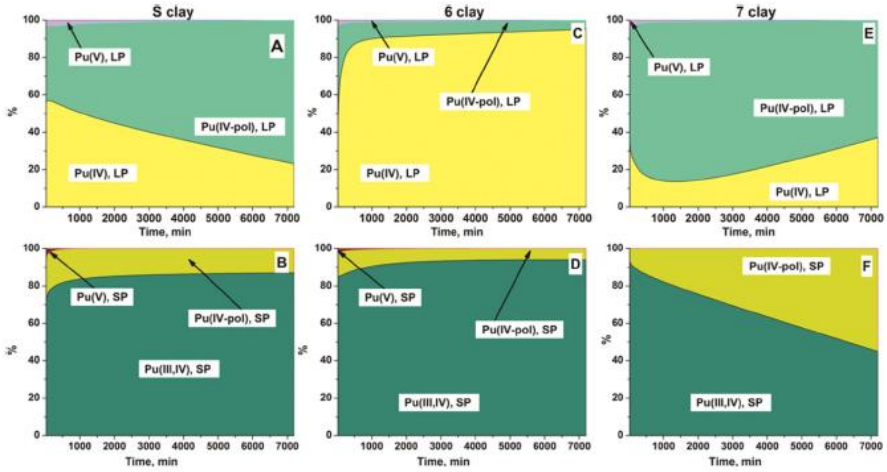

Fig. 3.19. Pu (V) oxidation state distribution in kinetic sorption experiments with clay (liquid-phase (LP) and solid phase (SP). Solid-phase clay, liquid-phase – groundwater (1:1000), [Pu(V)] =1x10^{-10}mol L^{-1}

The fast reduction of Pu (V) observed for all three clay types can be attributed to the iron-bearing minerals present in these clay samples. Although the content of iron minerals in clay 7 was below the detection limit determined by Mössbauer spectroscopy, a quite high content of structural Fe^{2+} was found in the samples (Fig. 3.15). In addition, humic substances present in the groundwater could be responsible for Pu (V) reduction in the liquid-phase.

Data of SE studies from two sets of experiments – with Pu (IV) and Pu (V) – are presented in Fig. 3.20. It can be seen that in experiments with Pu (V) the largest portion of Pu is bound to carbonate fractions in clay S (79±5) % and clay 6 (83±6) %. However, (57±40) % of Pu was associated with carbonates and (35±3) % bound to organic matter in the coating of clay 7. It should be noted that clay 7 contained a higher amount of calcite and organic matter as compared to clays S and 6. The observed distribution points out to different reduction mechanisms at the liquid-solid interface of the studied clays due to variations in the mineralogical composition of clay coatings and reflects complicated surface mediated redox reactions in the systems. Variations in kinetics and mechanisms of Pu (V) reduction in the studied systems with clay samples containing minerals siderite, clinochlore, montmorillonite and hematite can be responsible for the different Pu bonding to clay surfaces. It should be noted that these results are in agreement with our data obtained for Pu (V) in sorption experiments with bottom sediments from the Baltic Sea where a large portion of Pu was detected in carbonate fractions as well. Analysis of the Pu oxidation state distribution revealed the presence

of Pu (III) in the exchangeable and carbonate fractions of SE in bottom sediments. Since Pu (III) was also detected in the experiments with clay minerals (studies are in progress) a similar sorption mechanism can be supposed.

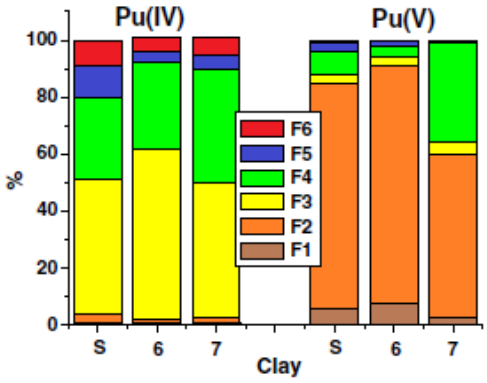

Fig. 3.20. Distribution of different binding forms of Pu (IV) and Pu(V) sorbed on clays after 7 days contact; F1 – exchangeable; F2 – carbonate bound; F3 – oxides, F4 – organic matter, F5 – acid soluble; F5 – residual

The obtained data revealed a different Pu bonding to clays in the sorption experiments with Pu (IV). Pu isotopes are mainly associated with oxides (47±3 % – 60±5 %) and organic matter (30±2 % – 40±3 %) (Fig.3.20). These variations can be explained by speciation of Pu (IV) and Pu (V) in liquid-phase as well as redox and sorption reactions with different components of solid-phase as discussed in the previous publications. Complicated behavior of Pu can be only partly explained on the basis of experiments performed with the pure phases since complicated mixtures exist in the environment. However, similar data obtained from experiments with the Triassic clay samples and bottom sediments from the Baltic Sea have shown that carbonate-oxide-organic matter-clay complex naturally present in the environment acts in a similar way. In addition, it seems that mobility of Pu (V) introduced into the environment should be higher not only in the aqueous systems but also in sediments. For this reason, Pu oxidation state distribution in radioactive waste releases should be controlled.

CONCLUSIONS

1. GO oxidation degree determines the attached modifier amount and the nanocomposite is more suitable for use in the liquid medium of the broader range of pH due to increased sorption efficiency by 25 %. The results obtained using the magnetic graphene oxide 2 (MGO2) nanocomposite for the removal of Am and Pu from solutions at pH from 5 to 9 showed that sorption efficiency exceeded 90 %.

2. The magnetic Prussian blue graphene oxide (MPBGO) nanocomposite selectively sorbs Cs (I) isotopes from liquid media even at high concentration of K^+, Na^+ and other competing ions. The efficiency of MPBGO nanocomposite to sorb of Cs (I) from seawater was 100 %, with a maximum sorption capacity of 362 ± 14 mg g^{-1}.

3. Graphite oxide is characterized by rapid kinetics when used as a sorbent to remove Co^{2+}, Cu^{2+}, Pb^{2+} and Ni^{2+} metals from a liquid media. The contact time of 20 minutes with the contaminated medium is sufficient for sorption of 95 % - Ni^{2+}, 92 % - Cu^{2+}, 96 % - Co^{2+} and 90 % - Pb^{2+}.

4. It was found that the chitosan graphene oxide (CSGO) and magnetic graphene oxide (MGO) nanocomposites are most suitable for the removal of Am and Pu from liquids with a wide pH range as compared with all studied sorbents. Sorption efficiency of Am and Pu isotopes from liquids exceeds 93 % for CSGO in the pH range from 3 to 6 and 94 % for MGO in the pH range from 5 to 9.

5. The results of this study have indicated a rather weak Pu (V) bonding to clay in spite of its fast reduction to Pu (IV) as well as it's even better sorption kinetics parameters and K_d values compared to those of Pu (IV). SE studies have shown its possible higher spreading in the environment since a large portion of Pu was associated with mobile fractions (exchangeable and carbonates). The obtained results can be used to predict sorption behaviour of Pu isotopes in the radioactive waste repository environment and helpful in application of natural clay in case of emergency.

REFERENCES

1. Ambashta R.D., Sillanpaa M. Water purification using magnetic assistance: a review. J. Hazard. Mater. 180, 2010, 38 – 49;
2. Arun T., Prakash K., Kuppusamy R., Justin Joseyphus R. Magnetic properties of Prussian blue modified Fe_3O_4 nanocubes. Journal of Physics and Chemistry of Solids 74, 2013, 1761 – 1768;
3. Avramenko V., Bratskaya S., Zneleznov V., Sheveleva I., Voitenko O., Sergienko V. Colloid stable sorbents for cesium removal: preparation and application of latex particles functionalized with transition metals ferrocyanides. J. Hazard Mater. 186, 2011, 1343 – 1350;
4. Beyki M.H., Bayat M., Miri S., Shemirani F., Alijani H. Synthesis, characterization, and silver adsorption property of magnetic cellulose xanthate from acidic solution: prepared by one step and biogenic approach. Ind. Eng. Chem. Res. 53, 2014, 14904 – 14912;
5. Brodie B.C. On the atomic weight of graphite. Philos. Trans. Roy. Soc. 149, 1859, 249 – 259;
6. Byung M.Y., Ho B.P. Comprehensive Membrane Science and Engineering. 1, 2017, 358 – 385;
7. Ca D.V., Cox J.A. Solid phase extraction of cesium from aqueous solution using sol-gel encapsulates cobalt hexacyanoferrate. Microchim. Acta. 147, 2014, 31 – 37;
8. Castaldo R., Lama G.C., Aprea P., Gentile G., Lavorgna M., Ambrogi V., Cerruti P. Effect of the oxidation degree on self-assembly, adsorption and barrier properties of nano-graphene, Microporous and Mesoporous Materials 260, 2018, 102 – 115;
9. Chen J., Yao B., Li C., Shi G. An improved Hummers method for eco-Friendly synthesis of graphene oxide. Carbon 64, 2013, 225 – 229;
10. Choppin G.R. Actinide speciation in the environment. J. Radioanal. Nucl. Chem. 273, 2007, 695 – 703;
11. Delchet C., Tokarev A., Dumail X., Toquer G., Barré Y., Guari Y., Guerin Ch., Larionova J., Grandjean A.. Extraction of radioactive cesium using innovative functionalized porous materials. RSC Adv. 2, 2012, 5707 – 5716;
12. Dragan E.S., Cocarta A.I., Dinu M.V. Facile fabrication of chitosan/poly(vinyl amine) composite beads with enhanced sorption of Cu^{2+}. Equilibrium, kinetics, and thermodynamics. Chemical Engineering Journal. 255, 2014, 659 – 669;

13. Dresselhaus M.S., Dresselhaus G. Intercalation compounds of graphite, Adv. Phys. 51, 2002, 1 – 186;
14. Dreyer D.R., Park S., Bielawski Ch.W., Ruoff R.S. The chemistry of graphene oxide. Chem. Soc. Rev. 39, 2010, 228 – 240;
15. Dreyer D.R., Todd A.D., Bielawski Ch.W. Harnessing the Chemistry of graphene oxide. Chem. Soc. Rev. 43, 2014, 5288 – 5301;
16. Egodawatte S., Datt A., Burns E.A., Larsen S.C. Chemical insight into the adsorption of chromium(III) on iron oxide/mesoporous silica nanocomposites. Langmuir 31, 2015, 7553 – 7562;
17. El-Kamash A.M., El-Gammal B., El-Sayed A.A. Preparation and evaluation of cerium(IV) tungstate powder as inorganic exchanger in sorption of cobalt and europium ions from aqueous solutions. Journal of Hazardous Materials 141, 2007, 719 – 728;
18. Fan C., Li K.,Wang Y., Qian X., Jia J. The stability ofmagnetic chitosan beads in the adsorption of Cu2+. RSC Adv. 6, 2016, 2678 – 2686;
19. Fan L., Luo C., Lv Z., Lu F., Qiu H. Removal of Ag^{+} fromwater environment using a novel magnetic thiourea-chitosan imprinted Ag^{+}. J. Hazard. Mater. 194, 2011, 193 – 201;
20. Fan L., Luo C., Sun M., Li X., Qiu H. Highly selective adsorption of lead ions by water-dispersible magnetic chitosan/graphene oxide composites. Colloids Surf. B Biointerfaces 103, 2013, 523 – 529;
21. Faustino P.J., Yang Y., Progar J.J., Brownell C.R., Sadrieh N., May J.C., Leutzinger E., Place D.A., Duffy E.P., Houn F., Loewke S.A., Mecozzi V.J., Ellison C.D., Khan M.A., Hussain A.S., Lyon R.C. Quantitative determination of cesium binding to ferric hexacyanoferrate: Prussian blue. J. Pharm. Biomed. Anal. 47 , 2008, 114 – 125;
22. Geim A. K., Novoselov K. S. The Rise of Graphene. Nat. Mater. 6, 2007, 183 – 191;
23. Geng B., Jin Z., Li T., Qi X. Preparation of chitosan-stabilized Fe0 nanoparticles for removal of hexavalent chromium in water. Sci. Total Environ. 407, 2009, 4994 – 5000;
24. Gómez-Navarro C., Weitz R.T., Bittne, A.M., Scolari M., Mews A., Burghard M., Kern K. Electronic Transport Properties of Individual Chemically Reduced Graphene Oxide Sheets. Nano Letters. 7 (11), 2007, 3499 – 3503;
25. Grangeon S., Vinsot A., Tournassat C., Lerouge C., Giffaut E., Heck S., Groschopf N., Denecke M.A., Wechner S., Schäfer T. The influence of natural trace element distribution on the mobility of radionuclides.

The exemple of nickel in a clay-rock. Applied Geochemistry 52, 2015, 155 – 173;
26. Guibal E. Interactions of metal ions with chitosan-based sorbents: A review. Separation and Purification Technology 38 (1), 2004, 43 – 74;
27. Hareema Saleem, Mobeen Haneef, Hina Y. Abbasi, Synthesis route of reduced graphene oxide via thermal reduction of chemically exfoliated graphene oxide. Materials Chemistry and Physics 204, 2018, 1-7;
28. Hea H., Klinowski J., Forsterb M., Lerf A. Chemical Physics Letters Volume 287, 1998, 1–2;
29. Hee-Man Y., Sung-Chan J., Sang Bum H., Kune-Woo L., Changhyun R., Yun Suk H., Bum-Kyoung S. Prussian blue-functionalized magnetic nanoclusters for the removal of radioactive cesium from water. Journal of Alloys and Compounds 657, 2016, 387 – 393;
30. Hofmann U., Holst R. The Acidic Nature and the Methylation of Graphit oxide. Ber. Dtsch. Chem. Ges. 72, 1939, 754 – 771;
31. Hovinga A.L., Sanderb M., Bruggemanc C., Behrendsa T. Redox properties of clay-rich sediments as assessed by mediated electrochemical analysis: Separating pyrite, siderite and structural Fe in clay minerals. Chemical Geology 457, 2017, 149 – 161;
32. Hu X.J., Liu Y.G., Wang H. Removal of Cu(II) ions from aqueous solution using sulfonated magnetic graphene oxide composite. Sep. Purif. Technol. 108, 2013, 189 – 195;
33. Hua M., Zhang S, Pan B., Zhang W., Lv L., Zhang Q. Heavy metal removal from water/wastewater by nanosized metal oxides: A review. J Hazard Materials 211 – 212, 2012, 317– 331;
34. Hummers W.S., Offeman R.E. Preparation of graphitic oxide. Journal of the American Chemical Society 80, 1958, 1339;
35. Hur J., Shin J., Yoo J., Seo Y.S. Competitive Adsorption of metals onto magnetic graphene oxide: comparison with other carbonaceous adsorbents. Scientific World J 11, 2015;
36. Ivanovskii A.L. Graphene-based and graphene-like materials. Russ. Chem. Rev. 81, 2012, 571 – 605;
37. Jana S., Saha A., Nayak A.K., Sen K.K., Basu S.K. Aceclofenac-loaded chitosan-tamarind seed polysaccharide interpenetrating polymeric network microparticles. Colloids And Surfaces B: Biointerfaces 105 (0), 2013, 303 – 309;
38. Jia W., Lu S. Few-layered graphene oxides as superior adsorbents for the removal of Pb(II) ions from aqueous solutions. Korean J. Chem. Eng. 31 (7), 2014, 1265 – 1270;

39. Johansson A., Widenkvist E., Lu J., Boman M., Jansson U. Fabrication of high aspect ratio Prussian blue nanotubes using a porous alumina template. Nano Lett. 5, 2005, 1603 – 1606;
40. Joshia R.K., Alwarappan S., Yoshimurac M., Sahajwallaa V., Nishinad Y. Graphene oxide: the new membrane material. Applied Materials Today 1, 2015, 1 – 12;
41. Kalantari K., Ahmad M.M. Rapid Adsorption of Heavy Metals by Fe_3O_4/Talc Nanocomposite and Optimization Study Using Response Surface Methodology. Int. J. Mol. Sci. 15, 2014, 12913 – 12927;
42. Kavitha K., Keerthi T., Mani T.T. Chitosan polymer used as carrier in various pharmaceutical formulations: Brief review. International Journal of Applied Biology and Pharmaceutical Technology 2 (2), 2011, 249 – 258;
43. Kooyman T., Buiron L., Rimpault G. A comparison of curium, neptunium and americium transmutation feasibility. Annals of Nuclear Energy 112, 2018, 748 – 758;
44. Kovtyukhova N.I., Ollivier P.J., Martin B.R., Mallouk T.E., Chizhik S.A., Buzaneva E.V., Gorchinskiy A.D. Layer-by-Layer assembly of ultra thin composite films from micron-sized graphite oxide sheets and Polycations. Chem. Mater. 11, 1999, 771 – 778;
45. Kraft A. On the discovery and history of Prussian blue. Bull. Hist. Chem. 33, 2008, 61 – 67;
46. Kumar A., Alwarappan S. Graphene-Based Materials. Science and technology, 2014;
47. Kumar S., Koh J. Physiochemical and optical properties of chitosan based graphene oxide bionanocomposite. International Journal of Biological Macromolecules 70, 2014, 559 – 564;
48. Kumar S., Nair R.R., Pillai P.B., Gupta S.N., Iyengar M.A.R., Sood A.K. Graphene oxide-$MnFe_2O_4$ magnetic nanohybrids for efficient removal of lead and arsenic from water. ACS Appl. Mat. Interf. 6, 2014, 17426 – 17436;
49. Kumar S., Pente A.S., Bajpai R.K., Kaushik C.P., Tomar B.S. Americium sorption on smectite-rich natural clay from granitic ground water. Applied Geochemistry 35, 2013, 28 – 34;
50. Li D., Zhang B., Xuan F. The sequestration of Sr(II) and Cs(I) from aqueous solutions by magnetic graphene oxides. J. Mol. Liq. 209, 2015, 508 – 514;
51. Li J., Zhang S., Chen C. Removal of Cu(II) and fulvic acid by graphene oxide nanosheets decorated with Fe_3O_4 nanoparticles. ACS Appl. Mat. Interf. 4(9), 2012, 4991 – 5000;

52. Liu X., Chen G.R., Lee D.J., Kawamoto T., Tanaka H., Chen M.L., Luo Y.K. Adsorption removal of cesium from drinking waters: A mini review on use of biosorbents and other adsorbents. Bioresour. Technol. 160, 2014, 142 – 149;
53. Liu Z., Wang H.S., Liu C., Jiang Y.J., Yu G., Mu X.D., Wang X. The first TDDFT and MCD studies of free base triarylcorroles: a closer Look into solvent-dependent UV–visible absorption. Chemical Community 48, 2012, 4743 – 4745;
54. Loos-Neskovic C., Ayrault S., Badillo V., Jimenes, B., Garnier, E., Fedoroff, M., Jones, D.J., Merinov, B. Structure of copper-potassium hexacyanoferrate (II) and sorption mechanisms of cesium. J. Solid State Chem. 177, 2004, 1817 – 1828;
55. Lu W., Li J., Sheng Y., Zhang X., You J., Chen L. One-pot synthesis ofmagnetic iron oxide nanoparticle-multiwalled carbon nanotube composites for enhanced removal of Cr(VI) from aqueous solution. J. Colloid Interface Sci. 505, 2017, 1134 – 1146;
56. Lujanienė G., Meleshevych S., Kanibolotskyy V., Šapolaitė J., Strelko V., Remeikis V., Oleksienko O., Ribokaitė K., Ščiglo T. Application of inorganic sorbents for removal of Cs, Sr, Pu and Am from contaminated solutions. J. Radioanal. Nucl. Chem. 282, 2009, 787 – 791;
57. Lujanienė G., Šapolaitė J., Amulevičius A., Mažeika K., Motiejunas S. Retention of cesium, plutonius and americium by engineered and natural barriers. Czechoslovak Journal of Physics, Vol. 56, 2006, 102 – 110;
58. Lujanienė G., Šemčuk S., Kulakauskaitė I., Mažeika K.,Valiulis D., Juškėnas R., Tautkus S. Sorption of radionuclides and metals to graphene oxide and magnetic graphene oxide. J. Radioanal. Nucl. Chem., 2015, 44 – 61;
59. Lujanienė G., Štamberg K., Pakštas V., Juškėnas R., Kulakauskaitė I., Šemčuk S., Mažeika K., Vopálka D. Study of Pu sorption behavior in natural clay. Journal of radioanalytical and nuclear chemistry, 304, 2015, 53 – 59;
60. Marcano D.C., Kosynkin D.V., Berlin J.M., Sinitskii A., Sun Z., Slessarev A., Alemany L.B., Lu W., Tour J.M. Improved synthesis of graphene oxide. ACS .Nano 4, 2010, 4806 – 4814;
61. Mauter M.S., Elimelech M. Environmental applications of carbon-based nanomaterials. Environ. Sci.Technol. 42 (16), 2008, 5843 – 5859;
62. Metwally S.S., Ayoub R.R. Modification of natural bentonite using a chelating agent for sorption of ^{60}Co radionuclide from aqueous solution. Applied Clay Science 126 , 2016, 33 – 40;

63. Missana T., Colas E., Grandia F., Olmeda J., Mingarro M., García-Gutierrez M., Munier I., Robinet J., Grivie M. Sorption of radium onto early cretaceous clays (Gault and PlicatulesFm). Implications for a repository of low-level, long-lived radioactive waste, Applied Geochemistry 86, 2017, 36 – 48;
64. Mohamed E.M., Ebitasem A.S., El-Khatib A.M., Soliman M.A., Elhassan A. Allam. Layer-by-layer assembly and functionalization of nanobentonite with nanopolyaniline and oleic acid to remove divalent Zn, Co,65Zn, and 60Co from water and radioactive wastewater. Ecotoxicology and Environmental Safety 145, 2017, 665 – 673;
65. Muzzarelli R.A., Ilari P., Tarsi R., Dubini B., Xia W. Chitosan from Asidia coerulea. Carbohydrate Polymers 25 (1), 1994, 45 – 50;
66. Nair R.R., Wu H.A., Jayaram N., Grigorieva I.V., Geim A.K. Unimpeded permeation of water through helium leak-tight graphene based membranes. Science 335, 2012, 442 – 444;
67. Nandi D., Basu T., Debnath S., Ghosh A.K., De A., Ghosh U.C. Mechanistic insight for the sorption of Cd(II) and Cu(II) from aqueous solution on magnetic mn-doped Fe(III) oxide nanoparticle implanted graphene. J. Chem. Engin. Data. 58(10), 2013, 2809 – 2818;
68. Norrfors K.K., Marsac R., Bouby M., Heck S., Wold S., Lützenkirchen J., Schäfer T. Montmorillonite colloids: II. Colloidal size dependency on radionuclide adsorption. Applied Clay Science 123, 2016, 292 – 303;
69. Norrfors K.K., Marsac R., Bouby M., Heck S., Wold S., Lützenkirchen J., Schäfer T. Montmorillonite colloids: II. Colloidal size dependency on radionuclide adsorption. Applied Clay Science 123, 2016, 292 – 303;
70. Novoselov K.S., Geim A.K., Morozov S.V., Jiang D., Zhang Y., Dubonos S.V., Grigorieva I.V., Firsov A.A. Electric field effect in atomically thin carbon films. Sci. 306, 2004, 666 – 669;
71. Ojovan M.I., Lee W.E. An Introduction to Nuclear Waste Immobilisation. Second edition, 2014;
72. Park J.H., Chang B.U., Kim Y.J., Seo J.S., Choi S.W., Yun J.Y. Determination of low (137)Cs concentration in seawater using ammonium 12-molybdophosphate adsorption and chemical separation method. J Environ. Radioact. 99(12), 2008, 1815 – 1820;
73. Pike M., Buesseler K.O., Breier C.F., Dulaiova H., Stastna K., Sebesta F. Extraction of cesium in seawater off Japan using AMP-PAN resin and quantification via gamma spectroscopy and inductively coupled mass spectrometry. J. Radioanal. Nucl. Chem. 296, 2013, 369 – 374;

74. Powell B.A., Fjeld R.A., Kaplan D.I., Coates J.T., and Serkiz S.M. $Pu(V)O_2^+$ adsorption and reduction on synthetic Goethite (α-FeOOH) and Hematite (α-Fe_2O_3), Env Sci Technol 39, 2005, 2107 – 2114;
75. Prakash A., Chandra S., Bahadur D. Structural, magnetic, and textural properties of iron oxide-reduced graphene oxide hybrids and their use for the electrochemical detection of chromium. Carbon 50, 2012, 4209 – 4219;
76. Ren Y., Abbood H.A., He F., Peng H., Huang K. Magnetic EDTA-modifiedchitosan/SiO2/Fe_3O_4 adsorbent: Preparation, characterization, and applicationin heavy metal adsorption. Chemical Engineering Journal, 226(0), 2013, 300 – 311;
77. Ren Y., Li N., Feng J., Luan T.,Wen Q., Li Z., Zhang M. Adsorption of Pb(II) and Cu (II) from aqueous solution on magnetic porous ferrospinel $MnFe_2O_4$. J. Colloid Interface Sci. 367, 2012, 415 – 421;
78. Rinaudo M. Chitin and chitosan: properties and applications. Progress in Polymer Science 31(7), 2006, 603 – 632;
79. Romanchuk A.Y., Slesarev A.S., Kalmykov S.N., Kosynkin D.V., Tour J.M. Graphene oxide for effective radionuclide removal. Phys. Chem. Chem. Phys.15, 2013, 2321 – 2327;
80. Roy E., Patra S., Kumar D., Madhurim R., Sharma P.K. Multifunctional magnetic reduced graphene oxide dendrites: Synthesis, characterization and their applications. Biosens. Bioelectron. 68, 2015, 726 – 735;
81. Sasaki T., Tanaka S. Magnetic separation of cesium ion using prussian blue modified magnetite, Chem.Lett. 41, 2012, 32 – 34;
82. Schniepp H.C., Li J.L., McAllister M.J., Sai H., Herrera-Alonso M., Adamson D.H., Prud'Homme R.K., Car R., Saville D.A., Aksay I.A. Functionalized Single Graphene Sheets Derived from Splitting Graphite Oxide. The Journal of Physical Chemistry B. 110 (17), 2006, 8535 – 8539;
83. Seung-Mok, L., Laldawngliana, C., Tiwari, D., Iron oxide nano-particles-immobilized-sand material in the treatment of Cu(II), Cd(II) and Pb(II) contaminated waste waters. Chem. Engin. J. 195–196, 2012, 103–111.
84. Shan C.S., Yang H.F., Han D.X., Zhang Q.X., Ivaska A., Niu L. Graphene/AuNPs/chitosan nanocomposites film for glucose biosensing. Biosens. Bioelectron. 25, 2009, 1070;
85. Sharma L.K., Rajesh S.M., Umrao R.K., Singh T.N., Experimental Evaluation of Geomechanical Behaviour of Bentonite-Sand Mixture for Nuclear Waste Disposal. Procedia Engineering 191, 2017, 386 – 393;

86. Singh V., Joung D., Zhai L., Das S., Khondaker S.I., Seal S. Graphene based materials: Past, present and future. Prog. Mater. Sci. 56, 2011, 1178–1271;
87. Singh V., Joung D., Zhai Lei.,Soumen D., Khondaker S.I., Seal S. Graphene based materials: Past, present and future. Progr. Mat. Sci. 56(8), 2011, 1178 – 1271;
88. Sitko R., Turek E., Zawisza B., Malicka E., Talik E., Heimann J., Gagor A., Feist B., Wrzalik R. Adsorption of divalent metal ions from aqueous solutions using graphene oxide. Dalton Trans. 42, 2013, 5682 – 5689;
89. Soldano C., Mahmood A., Dujardin E. Production, properties and potential of graphene. Carbon. 48(8), 2010, 2127 – 2150;
90. Song W., Shao D., Lu S. Simultaneous removal of uranium and humic acid by cyclodextrin modified graphene oxide nanosheets. Sci. China Chem. 57, 2014, 1291 – 1299;
91. Staudenmaier L. Verfahren zurdarstellung der graphit saure. Berichte der Deutschen Chemischen Gesellschaft 31(2), 1898, 1481 – 1487;
92. Sun Y., Ding C.,Cheng W. Simultaneous adsorption and reduction of U(VI) on reduced graphene oxide-supported nanoscale zerovalent iron. J. Hazard. Mat. 280, 2014, 399 – 408;
93. Sun Y., Wang Q., Chen C., Tan X., Wang X. Interaction between Eu(III) and graphene oxide nanosheets investigated by batch and extended X-ray absorption fine structure spectroscopy and by modeling techniques. Environ. Sci. Technol. 46, 2012, 6020 – 6027;
94. Thompson D.F., Church C.O. Prussian blue for treatment of radiocesium poisoning. Pharmacotherapy 21, 2001, 1364 – 13677;
95. Tournassat C., Grangeon S., Leroy P., Giffaut E. Modeling specific pH dependent sorption of divalent metals on montmorillonite surfaces. A review of pitfalls, recent achievements and current challenges. American Journal of Science 313, 2013, 395 – 451;
96. Tran H.V., Tran L.D. Preparation of chitosan/magnetite composite beads and their application for removal of Pb(II) and Ni(II) from aqueous solution. Mat. Sci. Eng. Mat. Sci. Eng. 2010, 304 – 310;
97. Ubara H., Yki E., Tsukiyama K., Kamizawa M., Senoh K., Ohta K., Shimamoto F., Ohta N. Treatment of water contaminated with radiocesium using novel complexes between Prussian-Blue and bivalent transition metal hydroxides. Trans. Atomic Energy Soc. Japan.13 (4), 2014, 127 – 135;
98. Vipin A., Hu B. Prussian blue caged in alginate/calcium beads as adsorbents for removal of cesium ions from contaminated water. J Hazard. Matter. 2013, 93 – 101;

99. Wang H., Yuan X., Wu Y., Huang H., Peng X., Zeng G., Zhong H., Liang J., Ren M.M. Graphene-based materials: Fabrication, characterization and application for the decontamination of wastewater and wastegas and hydrogen storage/generation. Adv. Coll. Interf. Sci. 195–196, 2013, 19 – 40;
100. Wang S., Sun H., Ang H.M., Tadé M.O. Adsorptive remediation of environmental pollutants using novel graphene-based nanomaterials. Chem. Engin. J. 226, 2013, 336 – 347;
101. Wenbao J.W., Lu S. Few-layered graphene oxides as superior adsorbents for the removal of Pb(II) ions from aqueous solutions. Korean J. Chem. Eng. 31(7), 2014, 1265 – 1270;
102. Wenqin W., Yan Y., Haihui Z. Highly efficient removal of Cu (II) from aqueous solution by using graphene oxide. Water Air Soil Pollut. 224, 2013, 1372 – 1375;
103. Wu W.Q., Yang Y., Zhou H.H., Ye T.T., Huang Z.Y., Liu R., Kuang Y.F. (2013) Highly efficient removal of Cu (II) from aqueous solution by using graphene oxide. Water Air Soil Pollut 224, 2013, 1372-1378;
104. Xiangxue W., Zhongshan C., Xiangke W. Graphene oxides for simultaneous highly efficient removal of trace level radionuclides from aqueous solutions. Sci. China Chem. 11, 2015, 1766 – 1773;
105. Xu H., van Deventer J.S.J. The geopolymerisation of alumino-silicate minerals. International Jurnal of Mineral Processes 59 (3), 2000, 247 – 66;
106. Yakun Z., Liangguo Y., Weiying X. Adsorption of Pb(II) and Hg(II) from aqueous solution using magnetic $CoFe_2O_4$-reduced graphene oxide. J. Mol. Liq. 191, 2014, 177 – 182;
107. Yang H., Li H., Zhai J., Sun L., Zhao Y., Yu H. Magnetic prussian blue/graphene oxide nanocomposites caged in calcium alginate microbeads for elimination of cesium ions from water and soil. Chem. Eng. J. 246, 2014, 10 – 19;
108. Zhang L., Zeng Y., Cheng Z. Removal of heavy metal ions using chitosan and modified chitosan: A review. Journal of Molecular Liquids 214, 2016, 175 – 191;
109. Zhang Y., Yan L., Xu W. Adsorption of Pb(II) and Hg(II) from aqueous solution using magnetic CoFe2O4-reduced graphene oxide. J. Mol. Liquids. 191, 2014, 177 – 182;
110. Zhao G., Li J., Ren X., Chen C., Wang X. Few-Layered graphene oxide nanosheets as superior sorbents for heavy metal ion pollution management. Environ. Sci. Technol. 45, 2011, 10454 – 10462;

111. Zhao H., Jiao T., Zhang L., Zhou J., Zhang Q., Peng Q., Yan X.. Preparation and adsorption capacity evaluation of graphene oxide-chitosan composite hydrogels. Sci. China. Mater. 58, 2015, 811 – 818;
112. Zhu Y., Murali S., Cai W., Li X., Suk J.W., Potts J.R., Ruoff R.S. Graphene and graphene oxide: synthesis, properties, and applications. Adv. Mater XX, 2010, 1 – 19;

FOR NOTES

FOR NOTES

Vilniaus universiteto leidykla
Universiteto g. 1, LT-01513 Vilnius
El. p. info@leidykla.vu.lt,
www.leidykla.vu.lt
Tiražas 12 egz.